NTNU – Trondheim
Norwegian University of
Science and Technology

Reliability-based Design of a Monopile Foundation for Offshore Wind Turbines based on CPT Data.

Ida Elise Overgård

Civil and Environmental Engineering
Submission date: June 2015
Supervisor: Gudmund Reidar Eiksund, BAT
Co-supervisor: Ivan Depina, BAT

Norwegian University of Science and Technology
Department of Civil and Transport Engineering

NORWEGIAN UNIVERSITY OF SCIENCE AND TECHNOLOGY
DEPARTMENT OF CIVIL AND TRANSPORT ENGINEERING

Report Title: Reliability-based Design of a Monopile Foundation for Offshore Wind Turbines based on CPT Data	Date: 09.06.2015 Number of pages (incl. appendices): 125				
	Master Thesis	X	Project Work		
Name: Ida Elise Vikestad Overgård					
Professor in charge/supervisor: Professor Gudmund Reidar Eiksund, NTNU					
Other supervisors: PhD. Candidate Ivan Depina, NTNU					

Abstract:

A reliability-based design optimization (RBDO) of a monopile foundation for offshore wind turbines is conducted to optimize monopile design criteria by explicitly accounting for the effects of uncertainties. The RBDO in this study aims at optimizing cost of construction, installation and failure with respect to the ultimate limit state of a monopile foundation while accounting for the effects of uncertainties in soil parameters and lateral loads.

Due to the inherent soil variability and measurement errors, a probabilistic link is constructed to model soil parameter interpretation from CPT data. The probabilistic link is composed of a random field model of CPT data and the interpretation uncertainty associated with existing relations between soil parameters and CPT measurements. Advanced maximum likelihood procedures were employed to account for the effects of spatial correlation in the random field parameters of CPT measurements.

Probabilistic models for soil parameters and lateral loads are coupled with the nonlinear p-y finite element model to predict the response of a monopile foundation. The response of a monopile foundation is evaluated with respect to the ultimate limit state, defined by the yield strength of the monopile steel. Based on uncertainties in soil parameters and lateral loads, the probability of exceeding the ultimate limit is evaluated with the Subset Simulation method. The RBDO problem is solved by coupling the Subset Simulation reliability method with the Simulated Annealing stochastic optimization algorithm to minimize the monopile design cost.

Keywords:

1. Reliability-based design optimization (RBDO)
2. CPT
3. Geostatistics
4. Random field theory
5. p-y model

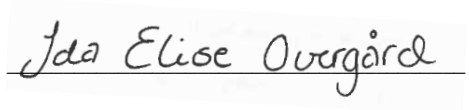

NTNU
Faculty of Engineering Science and Technology
Institute of Civil and Transport Engineering

MASTER DEGREE THESIS

Spring 2015
for

Student: Ida Elise Vikestad Overgård

Reliability-based design of a monopile foundation for offshore wind turbines based on CPT data

BACKGROUND

Inherent soil variability, measurement errors and modeling assumptions results in uncertainties in geotechnical design parameters. In a deterministic geotechnical design, characteristic values and the factor of safety approach are commonly used to maintain some degree of safety. In situations with high level of uncertainty probabilistic approaches are applied to quantify the effects of uncertainties on a geotechnical design.

A common source of uncertainty in geotechnical designs is the aleatory and epistemic uncertainty of soil properties. Uncertainties associated with soil properties are a combination of the inherent soil variability due to randomness in geological mechanisms involved in forming soil profiles and the uncertainties related to measurements and interpretation of soil properties. Uncertainties in soil properties can be modeled with a random field probabilistic model, capable of capturing point and spatial variability of soil properties. Point variability describes the uncertainties of a soil property on a single location within the soil domain. On the other hand, spatial variability represents the commonly observed decrease in similarity of soil measurements with the increase of spatial distance between measurement locations.

Reliability-based design optimization (RBDO) is a design framework which enables optimization of design performance criteria (e.g., cost, safety) while explicitly accounting for the effects of uncertainties in design parameters. The RBDO framework can be efficiently applied to quantify the effects of uncertainties on a geotechnical design.

TASK

The main task of this thesis is to conduct an RBDO of a monopile foundation for offshore wind turbines based on a probabilistic interpretation of soil parameters from CPT data. Soil parameters relevant for the design of monopile foundations are interpreted by a probabilistic link which integrates inherent variability of CPT data, measurement and interpretation uncertainties.

Task description

The probabilistic link between CPT data and interpreted soil parameters is constructed on a random field model of CPT data and existing relations between CPT measurements and soil parameters. Uncertainties in interpreted soil parameters are comprised of inherent variability of CPT data and

measurement and interpretation uncertainty associated with existing relations between CPT data and soil parameters.
A probabilistic model of soil properties is integrated within the RBDO framework to minimize cost of monopile construction, installation and failure while satisfying a reliability constraint. Reliability constraint, defined by a failure probability limit, expresses safety criteria for a monopile design. Reliability analysis is performed by coupling probabilistic models of soil parameters and random lateral load with the p-y finite element model simulating the response of a monopile foundation. Reliability analysis is conducted with respect to the ultimate limit state of a monopile defined by the monopile steel yield strength.

Objective and purpose
The objective of this thesis is to implement a consistent probabilistic framework for the interpretation of soil parameters from CPT data and to demonstrate advantages of the RBDO formulation in a geotechnical design.

Subtasks and research questions

Literature study on probabilistic models for CPT data and existing relations to soil parameters for a monopile design.

Implementation of a probabilistic link between CPT data and soil parameters relevant for the monopile design.

Soil parameter interpretation from CPT data from the Sheringham Shoal Offshore Wind farm.

RBDO of a monopile foundation based on the interpreted soil parameters from the Sheringham Shoal Offshore Wind farm.

Professor in charge: Gudmund Reidar Eiksund

Other supervisors: Ivan Depina

Department of Civil and Transport Engineering, NTNU
Date: 08.06.2015

Gudmund Eiksund
Professor in charge (signature)

Preface

This master thesis is a part of the Master of Science degree in Civil and Environmental Engineering at the Norwegian University of Science and Technology. The thesis was written over a course of 20 weeks, spring 2015. In this study, a reliability-based design of a monopile foundation for offshore wind turbines is conducted to quantify uncertainties in soil parameters based on CPT data. The idea behind this thesis was developed by my supervisors, Professor Gudmund Eiksund and PhD. Candidate Ivan Depina, and they deserve a great acknowledgment for their help and guidance.

A special thanks to Ivan Depina, which introduced me to the fields of geostatistics in a way that made me want to learn more about it. Thanks for always being motivating and positive, I am very grateful for all the help and advices I have received.

I would also like to thank NGI and StatoilHydro for allowing me to use the CPT measurements from Sheringham Shoal Wind Farm.

Working with this thesis would not have been the same without my co-students at the office. They deserve a huge gratitude for having contributed to a good environment, both socially and academically.

Trondheim, 2015-06-09

Ida Elise Vikestad Overgård

Abstract

A reliability-based design optimization (RBDO) of a monopile foundation for offshore wind turbines is conducted to optimize monopile design criteria by explicitly accounting for the effects of uncertainties. The RBDO in this study aims at optimizing cost of construction, installation and failure with respect to the ultimate limit state of a monopile foundation while accounting for the effects of uncertainties in soil parameters and lateral loads.

Due to the inherent soil variability and measurement errors, a probabilistic link is constructed to model soil parameter interpretation from CPT data. The probabilistic link is composed of a random field model of CPT data and the interpretation uncertainty associated with existing relations between soil parameters and CPT measurements. Advanced maximum likelihood procedures were employed to account for the effects of spatial correlation in the random field parameters of CPT measurements.

Probabilistic models for soil parameters and lateral loads are coupled with the nonlinear p-y finite element model to predict the response of a monopile foundation. The response of a monopile foundation is evaluated with respect to the ultimate limit state, defined by the yield strength of the monopile steel. Based on uncertainties in soil parameters and lateral loads, the probability of exceeding the ultimate limit is evaluated with the Subset Simulation method. The RBDO problem is solved by coupling the Subset Simulation reliability method with the Simulated Annealing stochastic optimization algorithm to minimize the monopile design cost.

Sammendrag

En sannsynlighetsbasert optimalisering for fundamentering av vindmøller offshore er gjennomført for å optimalisere designet av en monopele ved å hele tiden ta høyde for effekten av usikkerheter. Målet for oppgaven er å optimalisere kostnadene for konstruksjon, installasjon og svikt samtidig som effekten av usikkerheter knyttet til jordparametere og laster blir medregnet.

På grunn av de naturlige iboende variasjonene i jorden og feil knyttet til målinger, er det konstruert en sannsynlighetsbasert kobling for tolkning av jordparametere fra CPT data. Denne sannsynlighetsbaserte koblingen består av en Gaussian tilfeldig felt modell av CPT data og usikkerheter knyttet til eksisterende metoder for å tolke jordparametere fra CPT målinger. Maximum Likelihood Method er en avansert prosedyre som ble anvendt for å ta hensyn til den romlige korrelasjonen når CPT målinger blir betraktet som et tilfeldige felt.

Sannsynlighetsbaserte modeller for jordparametere og laster ble koblet sammen med den ikke-lineære p-y modellen for å kunne si noen om responsen av monopelen når den blir utsatt for horisontale laster. Responsen av monopelen er evaluert med hensyn til bruddgrensetilstanden, som i dette tilfellet er definert som flytespenningen til stålet i pelen. Basert på usikkerheter i jordparametere og horisontale laster, er sannsynligheten for å overskride grensetilstanden evaluert ved hjelp av sannsynlighetsmetoden Subset Simulation. Det sannsynlighetsbaserte optimaliseringsproblemet er løst ved å koble algoritmen for Subset Simulation sammen med den stokastiske optimaliseringsalgoritmen Simulated Annealing.

Contents

List of Figures

List of Tables

Nomenclature

Latin Symbols

Symbol	Explanation	Unit
a	Net area ration	[-]
A_c	Projected area of cone	[m^2]
A_n	Cross-section area of the load shaft area	[m^2]
b_k	Failure limit	
b_i	Intermediate failure limit	
$\mathbf{C}$	Correlation matrix	
C_i	Initial cost of production and installation	[€]
C_F	Failure cost	[€]
CoV_x	Coefficient of variation	
dl	Interval length	[m]
D	Pile diameter	[m]
E_p	Young's modulus of steel pile	[MPa]
E_{py}	Slope of p-y curve	[kPa]
E_s	Young's modulus of soil	[kPa]
f_s	Sleeve friction	[kPa]
F	Failure region	
F_i	Intermediate failure region	
F_s	Factor of safety	[-]
$G(\mathbf{x})$	Performance function	
H	Lateral load	[kN]
I_F	Indicator function	
J	Empirical model parameter	
k	Initial modulus of subgrade reaction	[MPa/m]

Symbol	Explanation	Unit
L_p	Pile embedded length	[m]
M	Bending moment	[kNm]
N_k	Empirical cone factor	[-]
N_s	Number of simulations	
p	Soil resistance	[kN/m]
p_u	Ultimate soil resistance	[kN/m]
P_F	Probability of failure	
P_F^{lim}	Reliability limit	
q_c	Cone tip resistance	[MPa]
Q_c	Total force acting on the cone	[kN]
q_t	Corrected cone tip resistance	[MPa]
S_u	Undrained shear strength	[kPa]
u_2	Total pore pressure behind the cone	[kPa]
w	Pile wall thickness	[m]
x_i	Random variable	
y	Deflection of pile	[m]
y_{50}	Deflection at one-half the ultimate soil resistance	[m]
z	Depth below seabed	[m]
z_w	Water depth	[m]

Greek Symbols

Symbol	Explanation	Unit
α_1	Linear trend parameter for mean value of random field	
α_2	Linear trend parameter for mean value of random field	
β_1	Linear trend parameter for standard deviation of random field	
β_2	Linear trend parameter for standard deviation of random field	
γ	Soil unit weight	[kN/m^3]
γ'	Submerged unit weight	[kN/m^3]
γ_w	Unit weight of water	[kN/m^3]
ε	Transformation uncertainty	
ε_{50}	Strain at one-half the ultimate soil resistance	[−]
θ	Correlation length	[m]
μ_x	Mean value	
μ_{q_t}	Mean value of corrected cone resistance	[MPa]
ρ_s	Density of steel	[kN/m^3]
ρ_{xy}	Correlation	
$\rho(\tau)$	Correlation between two points	
σ_{lim}	Steel yield stress	[MPa]
σ_x	Standard deviation	
σ_{v0}	Total overburden pressure	[kPa]
σ'_{v0}	Effective overburden pressure	[kPa]
σ_{q_t}	Standard deviation of corrected cone resistance	[MPa]
τ	Distance between two points	[m]
υ_s	Possons's ratio of steel	[-]
φ	Friction angle of soil	[°]
Ω	Domain	

Abbreviations

BCT	Botney Cut Formation
BDK	Bolders Bank Formation
CAUC	Consolidated anisotropically undrained traxial compression test
CIUC	Consolidated isotropic undrained traxial compression test
CK	Chalk Group
CPT	Cone Penetration Testing
CPTU	Cone Penetration Testing Undrained
EG	Egmond Ground Formation
MC	Monte Carlo
MCMC	Markov Chain Monte Carlo
NGI	Norwegian Geotechnical Institute
RBDO	Relatively-based Design Optimization
SA	Simulated Annealing
SS	Subset Simulation
SBK	Swarte Bank Formation
UU	Unconsolidated undrained triaxial compression
VST	Vane shear test

Chapter 1

Introduction

1.1 Background

Geotechnical design is prone to uncertainties due to inherent soil variability, measurement errors and modeling assumptions. How the uncertainties in soil properties affects the response of a foundation structure is of high interest, and has received considerable attention in the recent years. The idea of using statistical concepts in geotechnical engineering is not new, but the use of this methodologies has tended to be limited to projects relating to seismic design and offshore engineering (Fenton and Griffiths, 2008).

In deterministic geotechnical design, characteristic values and the factor of safety approach are commonly used to maintain some degree of safety. This approach is based on the ratio between expected strength of response to the expected load, which both are variables in practice. It is of importance to provide answers about the reliability of a design, and when the level of uncertainty is high, stochastic approaches becomes more necessary for system analyses and design.

The inherent soil variability is a consequence of irregular processes that has been ongoing for thousands of years. The physical properties of soil will vary within resulting deposits and result in point and spatial variability. Due to this, soil properties are shown to be spatially correlated. This distance, up to which the correlation between two points is significant, is defined as the correlation length. A probabilistic model commonly employed to characterize point and spatial variability of soil properties is known as the random field model.

Interpretation of soil parameters is usually a challenging task due to limited data, and the variability observed in measured data originates both from spatial variability and measurements errors. In the random field model contributions from these uncertainties are included and the model is thus sufficient for describing soil parameters in a probabilistic manner.

The random field approach is demonstrated by using a reliability problem of a monopile foundation. The local strength variation at a pile foundation is expected to have a greater effect compared to, for instance, a gravity-based foundation (Ronold, 1990). This is because the area exposed to soil for a pile foundation is significantly smaller and the response of laterally loaded piles are primarily determined by using p-y curves applied at nodal points between elements. In addition, the vertically correlation distance is significantly smaller than the horizontally and the uncertainty associated with soil properties requires a special consideration for this foundation design.

Problem Formulation

In this study, a reliability-based design optimization (RBDO) is conducted to quantify uncertainties in soil parameters based on CPT investigations. The interpretation of soil properties are based on a probabilistic link between the CPT measurement and soil design parameters.

Random field model is utilized to characterize point and spatial variability of CPT measurement. The Maximum likelihood method is implemented to estimate the vertical correlation length, mean value and standard deviation of cone resistance from available CPT measurements. These values are further used for a probabilistic soil parameter interpretation.

Monopiles are subjected to lateral loading. p-y curves describes the nonlinear relationship between the resistance acting on the pile wall, p, and the lateral deflection of the pile, y (Sørensen et al., 2012). The ultimate soil resistance, p_u, is an important parameter for construction of p-y curves. Undrained shear strength, S_u, is directly related to p_u, and the ultimate soil resistance for sand is calculated by dimensionless coefficients which depend on the friction angle, φ. Variability of S_u and φ are expected to have a significant influence on the pile-soil response and the point and spatial variability of these parameters are estimated by the random field model.

The last step will be to conduct a probabilistic analysis within the Markov Chain Monte Carlo framework to detect how uncertainties related to soil parameters and load effects the design of a monopile foundation. A RBDO algorithm will be used to minimize cost of the monopile design and account for reliability at the same time. This is done by coupling the Simulated Annealing with the Subset Simulation reliability algorithm. Simulated Annealing is a stochastic optimization technique which search for the minimum and rejects design parameters that returns a failure probability larger than the reliability limit of the structure. Subset Simulation calculates the failure probability, and the probabilistic response of the monopile foundation is obtained by coupling the p-y model with random load and random fields of S_u and φ.

Literature Study

This thesis contains several topics, which requires important literature from different sources. The available literature was sorted into groups from the beginning to get a good structure, and these main groups are Sheringham Shoal wind farm, geostatistics and random field theory, interpretation of CPT measurements, p-y method, reliability-based design and optimization. The most important sources from each group will be briefly described below.

The main source which made this study possible is the available CPT measurements from Sheringham Shoal wind farm. Almost 90 CPT measurements with penetration length of up to 50 m are available for interpretation. The geotechnical report from soil investigations at the wind farm site (Saue and Meyer, 2009) is also studied to obtain important information about the soil conditions at the wind farm site.

The background theory of geostatistics and random fields are mainly covered by the literature from Fenton and Griffiths (2008) and Baecher and Christian (2005).

Interpretation of CPT is widely discussed in the literature, but the uncertainties related to the commonly used transformation models are less discussed. To transform CPT measurements into design parameters approaches suggested by Lunne et al. (1997) are used, and the uncertainty related to these transformation models are taken from the study performed by Kulhawy et al. (1992) and Kulhawy and Mayne (1990).

To account for the effect of lateral load, monopiles are analyzed by p-y curves in the pile-soil soil model. This is the current practice and is also the method described in offshore standards DNV (2010) and API (2011).

The RBDO of a monopile foundation that is performed in this study is not much different from the one presented by Depina and Eiksund (2015). The main difference is that the probabilistic response of the monopile foundation is now simulated by coupling the p-y model with random field models of undrained shear strength and friction angle which are based on interpretation of measured CPT values.

All calculations in this study are performed by using MATLAB ® R2014a

1.2 Limitations

The variability of undrained shear strength is expected to influence the pile-soil response significantly due to the formulation of p-y curves for clay. For formulation of p-y curves for sand the variability of friction angle is expected to significantly influence the pile-soil response. The RBDO analysis in this study is limited to modeling uncertainties only in these two parameters, while the other soil parameters are assumed to be deterministic.

Data from the wind farm site shows that the Bolders Bank Formation (BDK), Egmond Ground Formation (EG) and Swarte Bank Formation (SBK) are of highest interest for construction of a monopile foundation. The ultimate soil resistance, which is an important parameter for constructing p-y curves, is varying with depth and depends on the soil type. BDK and SBK are characterized as stiff clay and EG is a sand layer, and only construction of p-y curves for these soil types are considered.

The main aim of this thesis is to develop a probabilistic link between CPT data and soil parameters such that these can be used as input parameters in a RBDO for a monopile foundation. Existing RBDO algorithms were used to conduct RBDO of a monopile foundation.

The RBDO is evaluated with respect to the ultimate limit state of monopile foundation, defined by the steel yield strength of the monopile.

1.3 Structure of the Report

Chapter 2 - Theoretical background where some of the basic statistic terms are shortly described. In this chapter also some theory behind cone penetration testing, monopile foundation and the p-y method are introduced. Description of soil conditions at the wind farm site and some principal limit state categories for offshore installation is also presented.

Chapter 3 - In this chapter an introduction to geostatistics and random field theory is provided. The factor of safety versus a reliability-based design is presented, and a description of the algorithm used for the reliability-based design optimization is introduced.

Chapter 4 - Parameter estimation for the random field model based on CPT measurements is described in this chapter. Some previous work is presented and the maximum likelihood method is implemented to estimate the vertical correlation length, mean value and standard deviation of random fields from CPT .

Chapter 5 - The random field generation for undrained shear strength and friction angle is described in this chapter.

Chapter 6 - In this chapter the input parameters and the results from the reliability-based design optimization is presented.

Chapter 7 - Discussion of results from advanced estimation of random field parameters, probabilistic soil parameter interpretation and the reliability-based design optimization.

Chapter 8 - In the last chapter the thesis is summarized and some recommendations for further work are given.

Chapter 2

Theoretical Background

2.1 Basic Statistics

Some of the basic statistic terms that is used later in this thesis are simply described below to give an introduction of statistical approaches.

2.1.1 Random Variable

An independent variable that can take a series of possible outcomes, each outcome with a certain probability or frequency, is denoted as a random variable (Huber, 2013). The random variable can either be discrete or continuous. Discrete means that the random variable has a countable set of outcomes, like the results of a dice throw. Continuous random variable takes values on the continuous scale, like the value of undrained shear strength of clay.

2.1.2 Mean Value, Standard Deviation and Coefficient of Variation

The mean, which is also the expected value of the random variable, is the center of gravity of the frequency distribution along the x-axis (Baecher and Christian, 2005). In other words, the mean value is the average of a set of data and is often denoted as

$$\mu_x = E(x) = \frac{1}{n}\sum_{i=1}^{n} x_i \tag{2.1}$$

A measure that is used to quantify the amount of variation or dispersion of a set of data values is the standard deviation. A standard deviation close to zero indicates that the data points tend to be very close to the mean value, while a high standard deviation indicates that the data points are spread over a wider range of values. The standard deviation of a set of data $\mathbf{x} = \{x_i, ..., x_n\}$, denoted as σ_x is:

$$\sigma_x = \sqrt{E[(X - \mu_x)^2]} = \sqrt{\frac{1}{n}\sum_{i=1}^{n}(x_i - \mu_x)^2} \tag{2.2}$$

Sometimes the dominator (n-1) is used rather than (n). This is done to correct a statistical bias, due to the fact that the mean also needs to be estimated from the same data.

The coefficient of variation, CoV_x, is defined as the ratio of the standard deviation to the mean:

$$CoV_x = \frac{\sigma_x}{\mu_x} \tag{2.3}$$

2.1.3 Common Distributions

There is several models that describes the distribution of random variables. The most commonly used models for continuous random variables are the normal distribution and the lognormal distribution.

Normal Distribution

The normal distribution, which is also known as the Gaussian distribution, is the classic bell-shaped function that is symmetric around the mean value. The tail of the curve decays in an exponential manner, with the decay rate dependent on the value of the standard deviation. There is a 68 percent chance that a normal variable will be within $\pm$ 1σ from the mean value, 95 percent chance that it will be within $\mu \pm 2\sigma$ and 99,7 percent that the value will be within $\mu \pm 3\sigma$. This means that it is very unlikely to observe a value that is outside $\pm 3\sigma$ from the mean value, as shown in Figure 2.1.

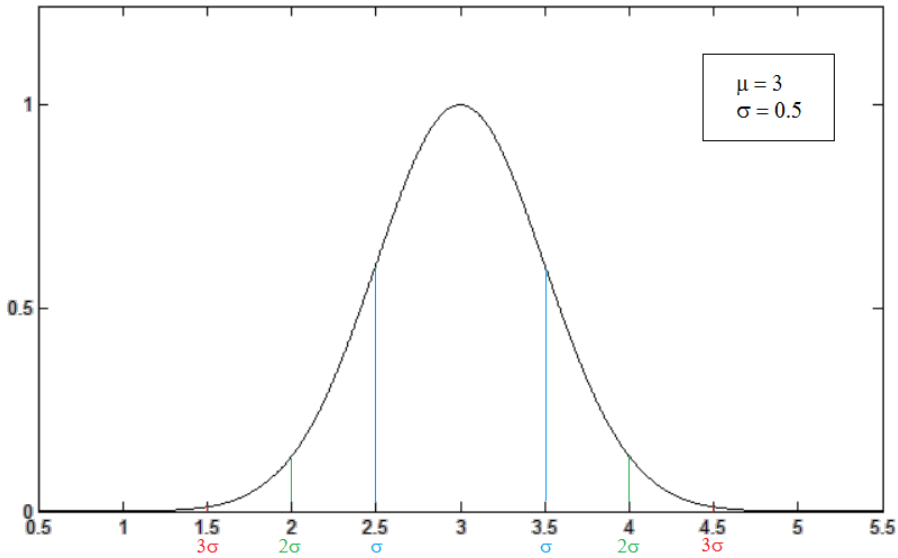

Figure 2.1: Normal distribution

The probability density function of a random variable, x, is given by Eq. 2.4.

$$f(x;\mu_x,\sigma_x) = \frac{1}{\sigma_x\sqrt{2\pi}} \times e^{-\frac{(x-\mu_x)^2}{2\sigma_x^2}} \tag{2.4}$$

Lognormal Distribution

A random variable will have a lognormal distribution if the logarithm of the variable is a normally distributed random variable. A lognormal distribution does not allow negative values of a variable. Since many geotechnical properties are non-negative, the lognormal distribution is a reasonable model in many cases. The probability density of a normal distribution is given by Eq. 2.5.

$$f(x;\mu_{lnx},\sigma_{lnx}) = \frac{1}{x\sigma_{lnx}\sqrt{2\pi}} \times e^{-\frac{(lnx-\mu_{lnx})^2}{2\sigma_{lnx}^2}} \tag{2.5}$$

Where μ_{lnx} and σ_{lnx} is given by:

$$\mu_{lnx} = ln\left(\frac{\mu_x}{\sqrt{1+\frac{\sigma_x^2}{\mu_x}^2}}\right) \tag{2.6}$$

$$\sigma_{lnx} = \sqrt{ln\left(1+\frac{\sigma_x^2}{\mu_x^2}\right)} \tag{2.7}$$

Gumbel Distribution

The Gumbel Distribution, which is also known as the extreme value distribution, is a widely applied statistical distribution for engineering problems. The distribution is commonly used to represent the distribution of the maximum by using daily, monthly or annual maximum values. The distribution is thus sufficient for estimating extreme values of waves. Figure 2.2 shows an example of a Gumbel distribution for a random variable with $\mu_x = 2500$ and $\sigma_x = 500$.

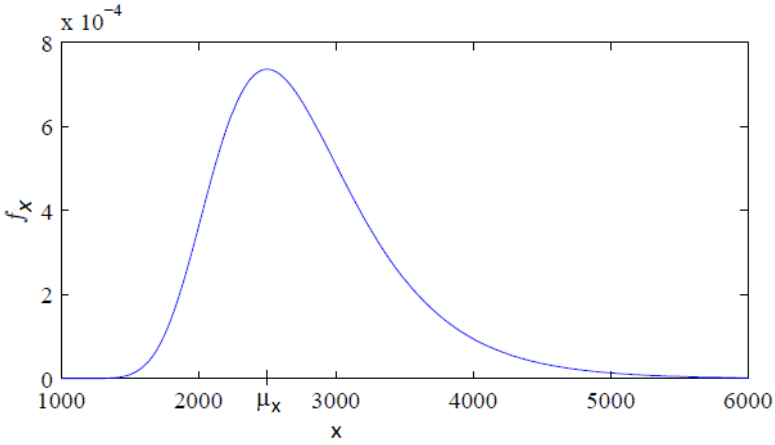

Figure 2.2: Gumbel distribution (after Depina and Eiksund, 2015)

2.2 Sheringham Shoal Windfarm

Sheringham Shoal is a wind farm site which is located approximately 20 km north of the Norfolk Coast, Offshore UK. The water depth at the site is around 20 m, thus should monopile foundation be a good solution for this site. The soil conditions described below are taken from the geotechnical report from soil investigations at the wind farm site (Saue and Meyer, 2009).

2.2.1 Description of Soil Conditions

Five main soil units were identified from seabed and down to a depth of 50 m; Botney Cut Formation (BCT), Bolders Bank Formation (BDK), Egmond Ground Formation (EG), Swarte Bank Formation (SBK) and the Chalk Group (CK). This was based on results from borings, samplings and CPTUs at the wind farm site, and some of the key parameters from each soil unit is summarized in Table 2.1.

Table 2.1: Soil parameters at Sheringham Shoal (after Saue and Meyer, 2009)

Soil Unit	Depth interval[1] [m]	Unit Weight γ [kN/m^3]	Undrained Shear strength S_u [kPa]	Friction Angle φ'_u [deg]
BCT	0 - 5	17	20 - 60	[-]
			varies [2]	
BDK	0 - 12	21.3	0 - 250	40.5
	7 - 12		varies [2]	36.0
EG	7 - 18	20.3	[-]	44
SBK	15 - 40	21.2	200 - 1100	33.5
	40 - 62	20	varies [2]	
CK	10 - 70	19.5	220 - 950	35.5 - 41.0
			varies [2]	varies [3]

[1] typical depth range based on borehole logs

[2] min-max S_u values quoted.

[3] varies with CK Grade

Table 2.1 shows that the Bolders Bank Formation, Egmond Ground Formation and Swarte Bank Formation are of highest interest for construction of a monopile foundation, and will be further described below. These layers are all heavily overconsolidated due to the geological history of the area which includes repeated glaciation.

Bolders Bank Formation

The Bolders Bank Formation is in the report described as firm to stiff slightly gravelly clay with pockets of sand and gravel. Sand layers with thickness of up to several meters have been encountered in the Bolders Bank Formation. The presence of sand layers and the variable composition of glacial deposits layers results in some scatter in the finest content data, but a characteristic fines content of 62 % is suggested.

Egmond Ground Formation

Egmond Ground Formation is described as very dense fine sand with locally seams and layers of silt and clay.

Swarte Bank Formation

Swarte Bank Formation is hard to very hard gravelly clay, where the gravel fraction comprising fine to medium size rounded to subrounded praticles of chalk. Such as for the Bolders Bank Formation, sand layers with thickness of up to several meters can be encountered in this formation.

2.3 Cone Penetration Testing

Due to the large quantity of available data from Sheringham Shoal wind farm, a RBDO of a monopile foundation is performed by interpreting CPT measurements. CPT is relatively inexpensive and a simple technique which provides near continuous measurements of soil properties.

CPT, a cone at the end of a series of rods is pushed into the ground. The rate of penetration is constant and continuous or intermittent real time measurements of cone resistance, q_c, and sleeve friction, f_s, are made. Cone penetration test undrained (CPTU) is cone penetration test with pore pressure measurements during penetration of the probe.

2.3.1 Cone Tip Resistance

Among the CPT measurements, the cone tip resistance is commonly used for soil parameter interpretation. The cone resistance is calculated as the total force acting on the cone, Q_c, divided by the projected area of the cone, A_c. Because of the wide use of CPT in geotechnical engineering practice, a great demand for validated correlations between cone resistance and engineering properties of soil have been developed.

2.3.2 Corrected Cone Tip Resistance

The conical tip has to be separated from the rest of the probe by a joint because it is demountable, and during penetration a pore pressure acting on this joint will be developed. Because of different end areas of the probe components on the two opposite sides of the joint, an unbalanced force will be produced. This results in too small recordings of the cone resistance, and this effect has to be accounted for. A corrected cone resistance is calculated by using Eq. 2.8.

$$q_t = q_c + (1 - a)\, u_2 \tag{2.8}$$

where:
q_t = corrected cone resistance [MPa]
q_c = recorded cone resistance [MPa]
u_2 = total pore pressure behind the cone [kPa]

a = $\frac{A_n}{A_c}$ is the net area ratio and is dependent on the probe design, where A_n is the cross-sectional area of the load cell or shaft and A_c is the projected area of the cone, as shown in Figure 2.3. Many cone penetrometers have values of cone area ratios ranging from 0.55 to 0.9 (Lunne et al. (1997)). For interpretation of CPTU measurements from Sheringham Shoal a net area ratio of 0.75 is assumed.

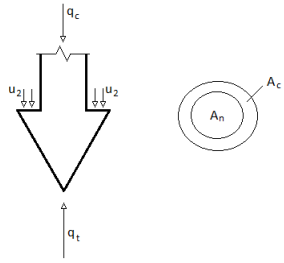

Figure 2.3: Corrected cone resistance

2.4 Monopile Foundations

Wind power is a renewable energy source, and as space is becoming scarce for the installation of onshore wind turbines, offshore windmills becomes important structures for continuing utilizing this energy resource in a good way. There are also other advantages to offshore wind energy compared to onshore. Stronger winds offshore imply greater productivity that may offset higher installation and operation costs (Breton and Moe, 2009).

There are also several challenges met by offshore wind. These structures are exposed to alternative loading from both wind and waves, which requires higher investments in towers, foundations and underwater cabling. The installation is also more difficult and expensive compared to onshore turbines. One foundation solution for these kinds of structures at moderate water depths is monopiles, which are single steel pipe piles driven open-ended into the soil. When planning the design of monopiles it is important to take into account that the structures are dominantly subjected to lateral loads and overturning moments, as shown in Figure 2.4.

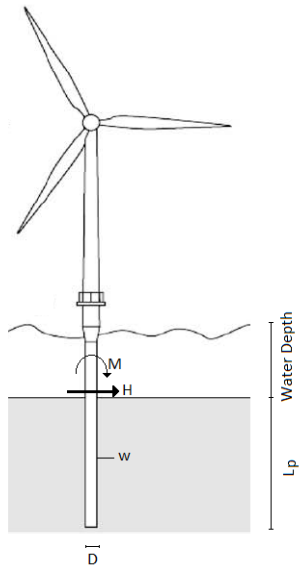

Figure 2.4: Monopile foundation for offshore wind turbines

The pile penetration depth, L_p, can be adjusted such that it suits the actual environmental and soil conditions at each location. A possible disadvantage of the monopile foundation design is too high flexibility in deep waters, and thus the monopile support structure is best suited for sites with water depth ranging from 0 to 25 meters.

To perform a design of a monopile foundation, two groups of uncertainties should be considered: loading conditions and resistance. Uncertainty about loading condition have to do with operational loads, accidental loads and environmental loads such as wind, waves and currents. Uncertainties about resistance have to do with site conditions, dynamic and static soil properties and how the monopile behaves when subjected to load (Baecher and Christian, 2005). The response of the monopile foundation to loads can be simulated by the p-y model.

2.4.1 P-Y Model

A p-y curve describes the non-linear relationship between the soil resistance acting on the pile wall, p, and the lateral deflection of the pile, y (Sørensen et al., 2012). This method, also known as the Winkler approach, is therefore able to produce a more accurate solution of the pile-soil response. The p-y curve method is developed and verified for small diameter, slender piles. In current practice and in offshore design codes (DNV (2010) and API (2011)) monopiles are analyzed with the p-y method, although these are large-diameter, non-slender piles.

In the Winkler approach the pile considered is supported by a series of uncoupled non-linear springs, as shown in Figure 2.5. Each spring has a stiffness E_{py_i}, defined as the secant modulus of the p-y curve.

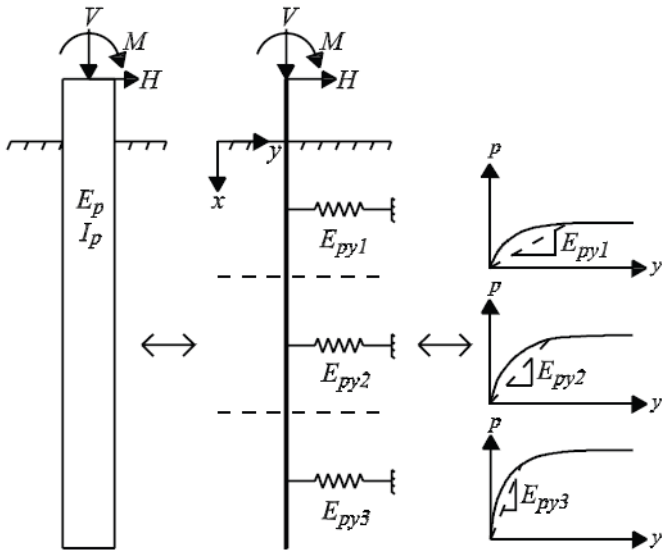

Figure 2.5: Pile modeled as an elastic beam supported by non-linear uncoupled springs under lateral loading (from Sørensen et al., 2012)

As we can see from Figure 2.5, the stiffness is increasing with depth and decreasing with increasing level of deflection, y. The curves also shows that after a certain y, the resistance is constant for increasing y and the soil behaves entirely plastic. This value is the ultimate soil resistance, p_u, which is varying with depth and will depend on the governing type of failure mechanism.

2.4.2 Construction of p-y Curves

The non-linear springs that is applied at the nodal points between the elements are characterized by p-y curves. Each nodal point is assumed to be uncoupled, which means that each spring is represented by its own ultimate soil resistance.

The ultimate soil resistance, p_u, is an important parameter when constructing p-y curves and how it is calculated depends on the soil type and the type of load. In this study only the static loading for stiff clay and sand under water will be further described below, because these equations are used later for the reliability-based design optimization.

Stiff clay under water - Static

The construction of p-y curves for piles in stiff clay was proposed by Reese et al. (1975) after studying the results from full scale test on laterally loaded piles in stiff clay in Manor, Texas. They recommend to calculate the static ultimate lateral resistance as:

$$p_u = \begin{cases} 2S_u D + \gamma' D z + 2.83 S_u z & \text{for } 0 < z \leq z_R \\ 11 S_u D & \text{for } z > z_R \end{cases} \tag{2.9}$$

where z is depth below seabed and z_R is the transition depth, below which the value of $2S_u D + \gamma' D z + 2.83 S_u z$ exceeds $11 S_u D$. S_u is the average undrained shear strength within the element, D is the pile diameter and γ' is the submerged unit weight.

For construction of the p-y curve we also need to calculate the deflection at one-half the ultimate soil resistance, y_{50}

$$y_{50} = \varepsilon_{50} D \tag{2.10}$$

where ε_{50} is the strain at one-half the ultimate soil resistance.

Figure 2.6 illustrates the characteristic shape of p-y curve for stiff clay during static loading and the construction of the curve is done by using Eq. 2.11

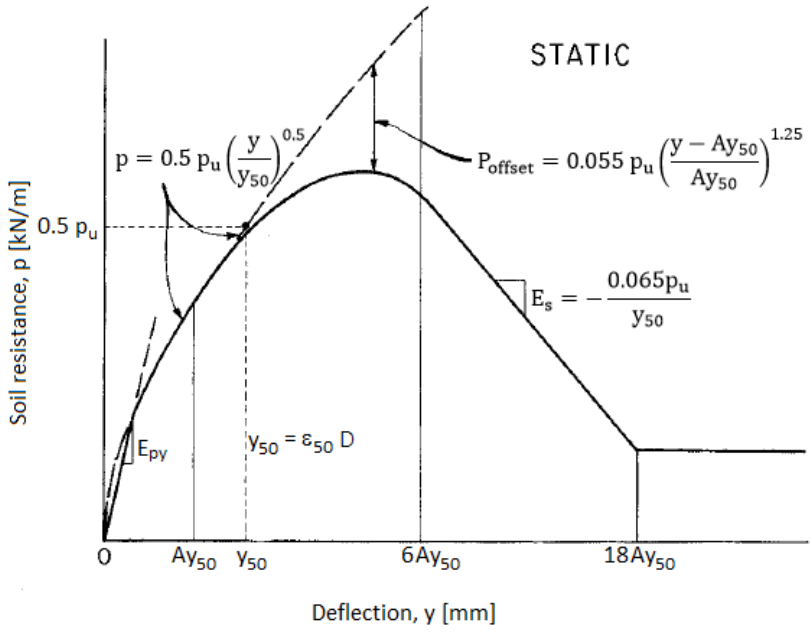

Figure 2.6: Characteristic shape of p-y curve for stiff clay during static loading (after Reese et al., 1975)

$$p = \begin{cases} 0.5 p_u \left(\frac{y}{y_{50}}\right)^{0.5} & \text{for } \frac{y}{y_{50}} \le A \\ 0.5 p_u \left(\frac{y}{y_{50}}\right)^{0.5} - 0.055 p_u \left(\frac{y - Ay_{50}}{Ay_{50}}\right)^{1.25} & \text{for } A < \frac{y}{y_{50}} \le 6A \\ 0.5 p_u (6A)^{0.5} - 0.411 p_u - \frac{0.0625}{y_{50}} p_u (y - 6Ay_{50}) & \text{for } 6A < \frac{y}{y_{50}} \le 18A \\ 0.5 p_u (6A)^{0.5} - 0.411 p_u - 0.75 p_u A & \text{for } \frac{y}{y_{50}} > 18A \end{cases} \tag{2.11}$$

where A is a non-dimensional coefficient, and the value of A is taken from Figure 2.7. Eq. 2.12 shows how the value of A is calculated.

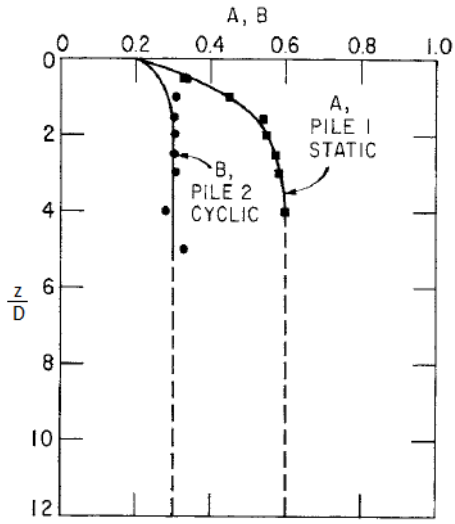

Figure 2.7: Non-dimensional coefficients used for construction of p-y curves, where coefficient A is for static loading (from Reese et al., 1975)

$$A = \begin{cases} -0.0011\left(\frac{z}{D}\right)^4 + 0.0193\left(\frac{z}{D}\right)^3 - 0.1223\left(\frac{z}{D}\right)^2 + 0.3532\left(\frac{z}{D}\right) + 0.2 & \text{for } \dfrac{z}{D} < 3.5 \\ 0.6 & \dfrac{z}{D} \geq 3.5 \end{cases} \tag{2.12}$$

Sand under water - Static

O'Neill and Murchison (1983) suggested a modified expression of the p-y curve for sand under water, which is also the formulation that is currently recommended by design codes (DNV (2010) and API (2011)). In the modified p-y curve formulation, the analytical expression for the ultimate soil resistance is approximated with dimensionless coefficients. These coefficients, C_1, C_2 and C_3, depend on the friction angle φ as shown in Figure 2.8, and the ultimate soil

resistance is recommended to be calculated as:

$$p_u = \begin{cases} (C_1 z + C_2 D)\gamma' z & \text{for } 0 < z \leq z_R \\ C_3 D \gamma' z & \text{for } z > z_R \end{cases} \tag{2.13}$$

where z is depth below seabed and z_R is the transition depth, below which the value of $(C_1 z + C_2 D)\gamma' z$ exceeds $C_3 D\gamma' z$. D is the pile diameter and γ' is the submerged unit weight of soil. The p-y curve can now be generated according to Eq. 2.14.

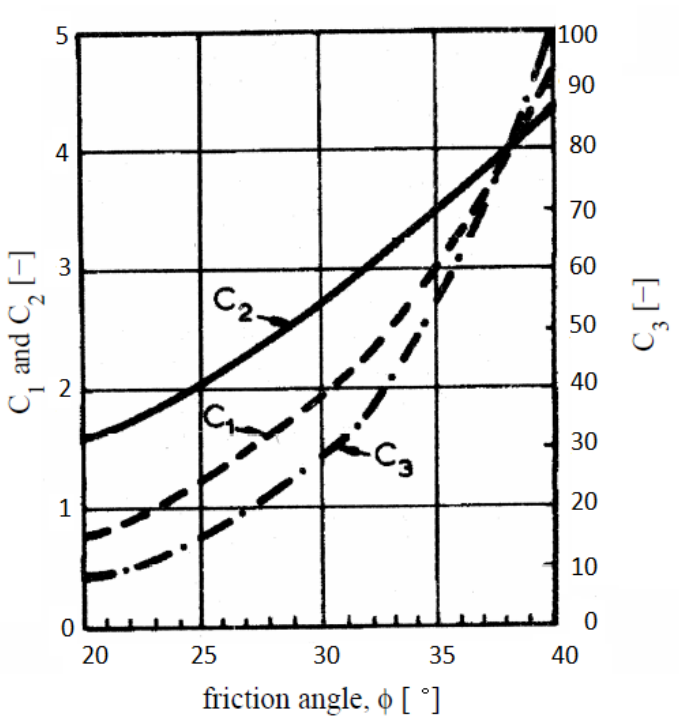

Figure 2.8: Non-dimensional coefficients as a function of friction angle used for calculating the ultimate soil resistance (after DNV, 2010)

$$p = Ap_u tanh\left(\frac{kz}{Ap_u} y\right) \tag{2.14}$$

where A is a factor that accounts for static or cyclic loading, and the value of A for static loading is given in Eq. 2.15, where k is the initial modulus of subgrade reaction and depends on the friction angle ϕ as shown in Figure 2.9.

$$A = \left(3 - 0.8\frac{z}{D}\right) \geq 0.9 \tag{2.15}$$

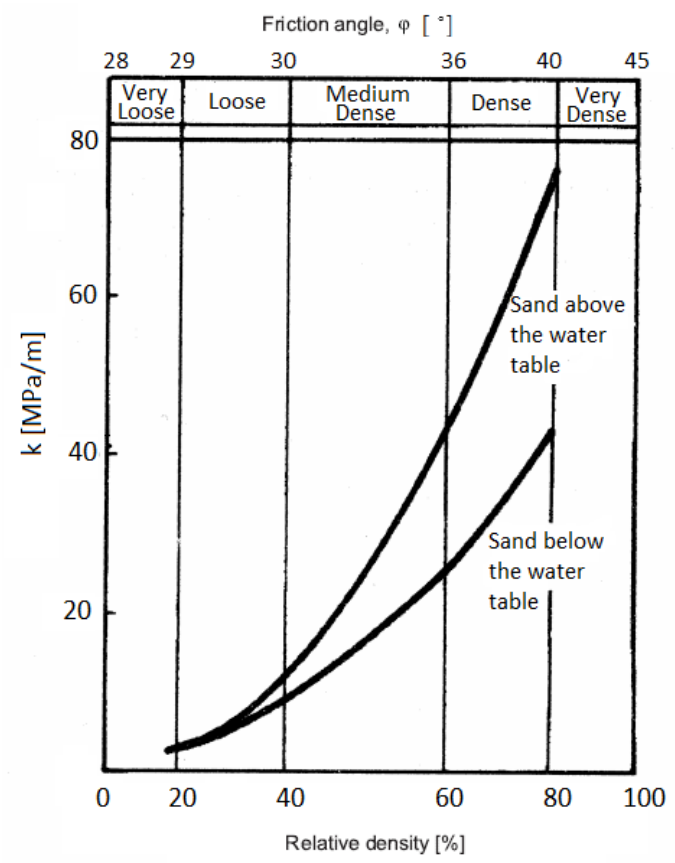

Figure 2.9: Variation of initial modulus of subgrade reaction k as a function of friction angle (after DNV, 2010)

2.5 Principal Limit State Categories for Offshore Installations

A limit state is defined as a state where the condition of the structure no longer fulfills the relevant design criteria. Beside the design for the maximum static load, fatigue design is also a very important aspect for offshore structures.

For monopiles the effect of cyclic pile response is a major design consid-

eration, because wind and wave loads all exhibit cyclic behavior. This type of loading leads to accumulated rotation of the wind turbine tower and adversely affect the ultimate strength and fatigue life of the wind turbine, including the supporting structure.

For monopiles it is also important to consider the serviceability limit state, which corresponds to factors such as deformations, vibrations and local damage that govern normal use. The monopiles are typically designed after deformation tolerance, which is often specified as a total rotation of the pile head in a vertical plane(Doherty and Gavin, 2012). The pile head is defined to be at the seabed and this criteria is typically derived from visual requirements.

If we consider the lifetime of the structure, the number of loads due to wind and wave could exceed 10^8 (Achmus et al., 2009). A safe design must therefore address issues of changes in stiffness due to long-term cyclic loading and rotation over time. This is not considered explicitly in the current codes and the recommended p-y curves for cyclic loading are designed primarily for evaluation of the ultimate lateral capacity. There is also considerable differences of opinion throughout the literature on the rate of cyclic displacement accumulation. This is one of the main reason why the reliability-based design optimization in this study only consider the ultimate limit state based on maximum static load.

Chapter 3

Geostatistics

3.1 Risk Assessment in Geotechnical Engineering

Inherent soil variability, measurement errors and modeling assumptions effects the uncertainties in geotechnical design. Estimation of soil parameters is usually a challenging task due to limited data, and traditionally this is solved by using characteristic values of soil properties. Further are these values used to determine a factor of safety for the design to maintain some degree of safety.

In this study we are interested in a probabilistic characterization of soil properties. How the uncertainties in soil properties effects the response of a foundation structure is of high interest, and it is important to provide answers about the reliability of a design.

3.1.1 Uncertainty

Uncertainties in soil properties are commonly a consequence of inherent soil variability and measurement data. Uncertainties in soil properties are generally divided into aleatory and epistemic uncertainty based on their origin.

Aleatory uncertainty

The physical properties of soils vary from place to place within resulting deposits because of irregular processes that has been ongoing for thousands of years. This natural variation is inherent and cannot be changed or eliminated.

Epistemic uncertainty

Epistemic uncertainty is associated with knowledge-based uncertainty, and can be reduced or eliminated. This knowledge-based uncertainty can be divided into three main areas (Lacasse and Nadim, 1997). First we have the statistical uncertainty, which is related to limited site investigation data. Secondly, measurement uncertainty which is related to determination of material parameters in the laboratory. Model uncertainty is the last area and is based on the uncertainty because of simplifications and idealizations made in the calculations. This uncertainty may be discovered by performing the calculations with different models.

3.1.2 Choosing a Distribution

In the reliability analyses of geotechnical structures, data obtained from field investigations are commonly used. One of the challenges in the analysis of these data is the determination of a suitable distribution. There will never be enough information, and this is why assumptions needs to be made based on the information that is obtainable. If there is sufficient data available, the distribution that best fits the histogram might represent the true distribution in a good way. Examples of how histograms of collected data of a random variable might look like are shown in Figure 3.1. The theoretical distribution that fit these observed data reasonably is selected as the distribution of the random variable.

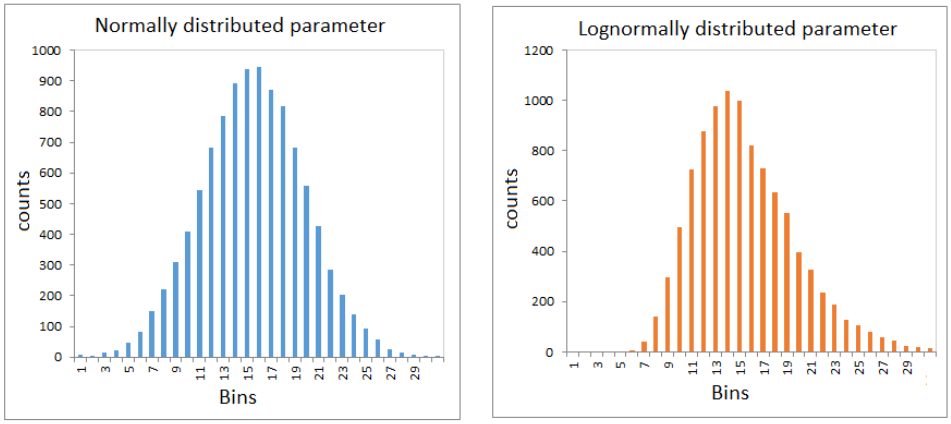

Figure 3.1: Histogram of collected data on an input variable of interest

One advantage by fitting a distribution to the collected data is that also the values outside the range of observed samples can be generated, which means that extreme values can be simulated from the distribution (Fenton and Griffiths, 2008). This is important because it is often the extremes that controls a design.

Within the field of geotechnical engineering it is important to ensure that the distribution is at least approximately physically reasonable. For instant, if a non-negative parameter is given a distribution that will return negative values with a relatively high probability, this is not considered as an appropriate distribution.

3.1.3 Maximum Likelihood Estimators

Many authors (e.g Fenton and Griffiths (2008) and Baecher and Christian (2005)) agree that a good approach to estimating the parameters of an assumed distribution is to find which parameter values lead to the greatest probability of observing those data. The maximum likelihood method finds the distribution parameters, also called maximum-likelihood estimators, which maximize the probability of observing these data.

3.1.4 Trend Analysis

The spatial variation of soil deposits can be characterized in detail, but only after a large number of test. In reality, the number of tests required far exceeds what can be acquired in practice.

In some cases may two data set have the same mean and standard deviation, but still describe different soil conditions. This is because the difference between data sets cannot always be inferred from the mean and standard deviation alone. By examine spatially dependent data, also known as a random or stochastic process, with trend analyses this can be solved. The trend analysis is conducted by separating the random process into a deterministic trend and a residual variability around the trend.

$$r(z) = t(z) + e(z) \tag{3.1}$$

where $r(z)$ is the soil property at location z, $t(z)$ is the value of the trend at z and

$e(z)$ is the residual variation

The residual variation is statistically characterized as a random process, usually with zero mean and non-zero variance. The variance of the residual reflects uncertainty between the interpolated trend and the actual value of soil properties at unobserved locations.

$$Var[e] = E[\{r(z) - (t(z))\}^2] \tag{3.2}$$

If the measured data shows a clear trend, this trend can be estimated by performing a regression analysis. This may reduce the variation of the measured data, but it is important to remember that this trend may not continue outside the sampling domain, D, as shown in Figure 3.2.

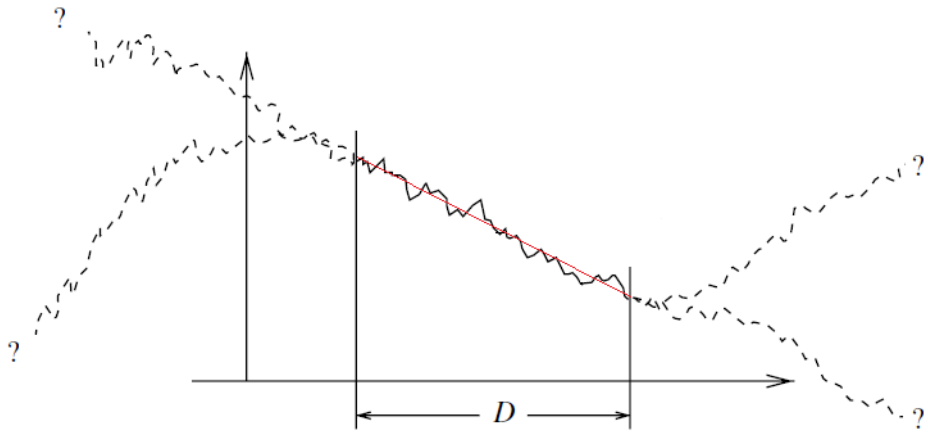

Figure 3.2: An observed trend may not continue outside the sampling domain, D

3.1.5 Local Average

For many geotechnical properties such as friction angle, elastic modulus, consolidation radio and shear modulus, a point value will not give a adequate value. Soils are actually discontinuous at the microscale (Fenton and Griffiths, 2008), and that is why soil property measurements are generally averaged over a volume.

3.2 Random Field and Spatial Variability

Soils are geological materials that have been subjected to various stresses, pore fluids, and physical and chemical changes. Even within soil layers that is nominally homogeneous, the engineering soil properties from point to point can exhibit considerable variations (Ronold, 1990). Our knowledge about soil properties is limited and the variability observed in measured data originates both from spatial variability and measurement errors. This is why spatial variability of soil properties can be modeled by using the mathematics of random processes, which is a collection of random variables.

Gaussian random fields and kriging are examples of techniques that are used for describing soil conditions in a probabilistic manner based on observed and measured data. The Gaussian random field model will be used later in this study and is described below.

3.2.1 Gaussian Process Theory

A stochastic process, with Gaussian finite dimensional distribution is a Gaussian process. Just as a Gaussian distribution is fully specified by its mean and covariance matrix, a Gaussian process is specified by a mean and covariance function (Fenton and Griffiths, 2008).

A Gaussian process is used for modeling dependent data observed over time or space and is commonly used to characterize the point and spatial variability of soil properties. A Gaussian process might also be known as a Gaussian random field. This continuous random field is defined by a multivariate normal distribution:

$$[R(x_1),...,R(x_2)] \sim N(\mathbf{x};\boldsymbol{\mu},\boldsymbol{\Sigma}) = \frac{1}{(2\pi)^{\frac{n}{2}}|\mathbf{C}|^{\frac{1}{2}}} \times exp\{-\frac{1}{2}(\mathbf{x}-\boldsymbol{\mu})^T\mathbf{C}^{-1}(\mathbf{x}-\boldsymbol{\mu}\} \quad (3.3)$$

Where $\mathbf{C} = E[(\mathbf{x}-\boldsymbol{\mu})(\mathbf{x}-\boldsymbol{\mu})^T]$ is the covariance matrix between the x's and is $n \times n$ symmetric. $|\mathbf{C}|$ is the determinant of $\mathbf{C}$ and $\boldsymbol{\mu} = E[\mathbf{x}]$ is the vector of mean values, one for each x_i,

For a continuous random field, the dimensions of $\boldsymbol{\mu}$ and $\mathbf{C}$ are sill infinite, since the random field is composed of an infinite number of x's, one for each point. To simplify things, we often quantify $\boldsymbol{\mu}$ and $\mathbf{C}$ using continuous functions of space based on just a few parameters.

Stationarity

Stationarity implies that the joint probability function is independent of spatial position and it depends only on relative position of the points. An assumption like this indicates that the mean, covariance and higher order moments are constant in time or space. This means that distinct trends in the mean or a variance that change with position is not found in the layer.

Autocorrelation

It is common to observe that the closer two measurement are located, the more similar the measured soil properties are. This type of spatial structure is examined through spatial correlations between soil properties. The spatial structure of soil remains in the residual and can be described by a spatial correlation, known as autocorrelation (Fenton and Griffiths, 2008). This concept of a statistical dependence between field values at different points is one of the major features of a random field representation of soil.

Correlation is a measure of dependence between two random variables commonly expressed with the linear correlation coefficient:

$$\rho_{xy} = \frac{Cov[X,Y]}{\sigma_x \sigma_y} \tag{3.4}$$

A autocorrelation represent a correlation of an individual variable with itself over space or time. The autocorrelation function describes the correlation coefficient between two measurements at distance τ, and is calculated as the covariance of the residuals at distance τ divided by the variation of the residuals.

$$\rho(\tau) = \frac{Cov[e(x_i), e(x_i)+\tau]}{Var[e(x_i)]} \tag{3.5}$$

It can be shown from observations that the correlation coefficients starts from ρ=1 at τ=0 and decays towards zero as the distance between the measurements increase. The correlation length θ is the distance within which points are significantly correlated.

Algorithm for generating Gaussian random fields

In reliability analyses the generated random field realizations are considered as an input to the model that simulate the response of the studied structure. A random field realization is generated by discretizing the domain into n points: $\mathbf{z} = (z_1, ..., z_n)$. Based on the discretization, a $n \times n$ covariance matrix is formulated. If we assume a stationary field, standard deviation is constant within the layer and the covariance matrix can be written as:

$$\mathbf{C} = \sigma_x^2 \begin{bmatrix} 1 & \rho(z_1, z_2) & .. & \rho(z_1, z_n) \\ \rho(z_2, z_1) & 1 & .. & \rho(z_2, z_n) \\ : & : & & : \\ \rho(z_n, z_1) & \rho(z_n, z_2) & .. & 1 \end{bmatrix} \tag{3.6}$$

This covariance matrix is decomposed in a lower $\mathbf{A}$ and a upper $\mathbf{A}^T$ triangular matrix with Cholesky decomposition.

$$\mathbf{C} = \mathbf{A}\mathbf{A}^T \tag{3.7}$$

To calculate the Gaussian random fields an $n \times 1$ vector of standard normal distributed random variables $\mathbf{T} \sim N(0,1)$ is generated. Gaussian random fields realization, $\mathbf{R}$, with the vector of means, $\boldsymbol{\mu}$, is generated:

$$\mathbf{R} = \boldsymbol{\mu} + \mathbf{A}\mathbf{T} \tag{3.8}$$

3.3 Factor of Safety

A common approach to deal with uncertainties in the engineering practice is known as the factor of safety approach. This is a semi-probabilistic design philosophy, and the main concern behind this approach is that is does not provide much physical insight into the likelihood of a design failure as a probabilistic measure (Fenton and Griffiths, 2008). The factor of safety is not a complete indicator of the safety margin because the uncertainty in parameters may affect the likelihood of failure significantly, as illustrated in Figure 3.3.

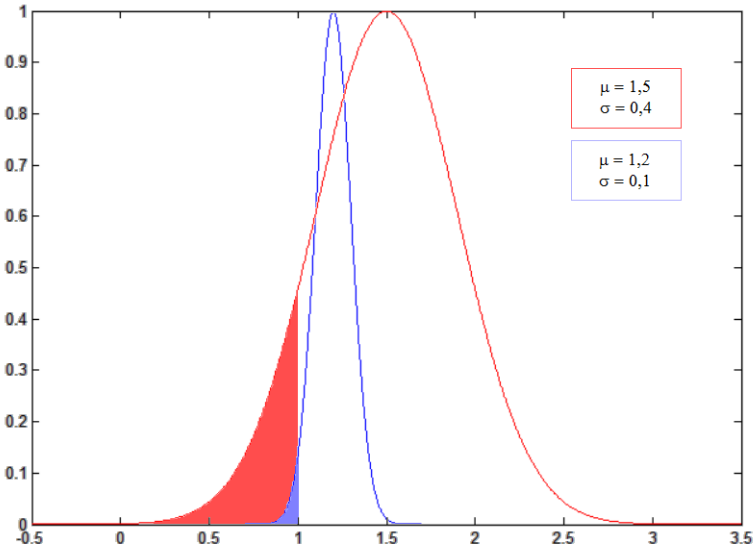

Figure 3.3: Probability density functions for different mean and standard deviation values for the factor of safety

Figure 2.3 shows two different distributions of the factor of safety, which is only selected for illustration. Because of large uncertainties in the case where $\mu = 1.5$ compared to the case where $\mu = 1.2$, the probability of failure ($P(F_s < 1)$) is larger for the case where the mean value of factor of safety is higher.

3.4 Reliability-based Design

In a reliability-based design, uncertain quantities such as load and resistance are represented as random variables and their corresponding distributions (Fenton and Griffiths, 2008). Compared to characteristic values and the factor of safety approach, probabilistic methods may give definite values for the probability of failure and costs related to risk reduction.

Probabilistic methods provides a tool to quantify the risk associated with projects, and gives us the opportunity to express the reliability of a design. It is important to emphasize that a reliability approach does not remove the uncertainty, but they do provide a way of handling them consistently. For instance, it will be possible to estimate how extensive the site investigations must be to achieve desired reliability in the results.

3.5 Reliability-based Design Optimization

A Reliability-based design optimization (RBDO) is a design methodology that accounts for uncertainty all along the optimization process. The concept is to optimize the structural performance criteria, such as cost, reliability and maintenance. This is done by explicitly accounting for the effects of uncertainties in the design process, such as material properties and loads.

The goal of a design optimization is to find the design parameters that minimizes the costs and satisfying some performance requirements at the same time. A RBDO problem can be forulated as shown in Eq. 3.9, where we want to minimize the design costs $C(\mathbf{x},\mathbf{t})$, which is a function of random parameters $\mathbf{x} = [x_1, x_2, ..., x_n]$ and design variables $\mathbf{t} = [t_1, t_2, ..., t_n]$.

$$C(\mathbf{x},\mathbf{t}) = C_i(\mathbf{t}) + C_F(\mathbf{t})P_F(\mathbf{x},\mathbf{t}) \tag{3.9}$$

$C_i(\mathbf{t})$ is the initial cost of the structure, C_F is the cost of failure and $P_F(\mathbf{x},\mathbf{t})$ represent the probability of failure.

3.5.1 Subset Simulation

One of the main goal of a reliability analysis is to evaluate the probability of an unsafe or undesired state of the structure. Unsafe or undesired state can be a property of the engineering system such as stress state or displacement limit. It is defined by the performance function $G(\mathbf{x},\mathbf{t})$, where $\mathbf{x} = [x_1, ..., x_n]$ represent the random parameters and $\mathbf{t} = [t_1, t_2, ..., t_n]$ represent design variables. The system is considered as unsafe when $G(\mathbf{x},\mathbf{t}) \leq 0$ and safe while $G(\mathbf{x},\mathbf{t}) \geq 0$. The probability of a structure being in this unsafe or undesired state is denoted as the probability of failure, P_F.

An unsafe or undesired state of the engineering system is often a rare event with very low probability of failure. Although the commonly used Monte Carlo method is accurate, robust and independent of the dimensionality of the reliability problem, the method is considered to be inefficient when small failure probabilities are evaluated. Subset simulation is then presented, where the basic idea about this method is to express the failure probability as a product of larger conditional failure probabilities. This is done by introducing intermediate failure events (Au and Beck, 2001).

Given a failure region F, let $F_1 \supset F_2 \supset ... \supset F_k = F$. F_i is the intermediate failure region and can be expressed by the performance function $G_i \leq b_i$, where $b_i > 0$ and $b_i, ..., b_k = 0$ defines the intermediate failure limits. This is illustrated in Figure 3.4.

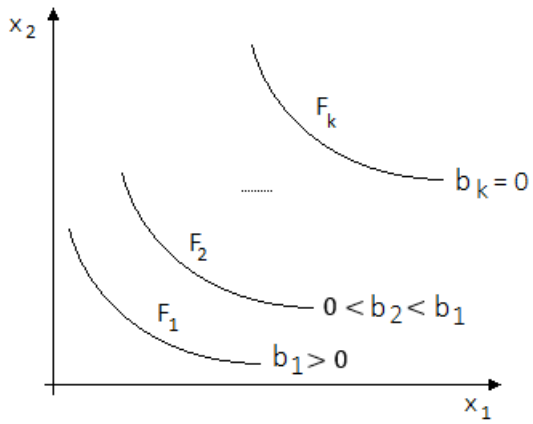

Figure 3.4: A set of intermediate failure events in Subset Simulation

The probability of failure is estimated by calculating the probability of being in the first intermediate failure region, $P(F_1)$, and conditional probabilities $\{P(F_{i+1}|F_i) : i = 1, ..., k-1\}$. This gives us the failure probability:

$$P_F = P(F_1) \prod_{i=1}^{k-1} P(F_{i+1}|F_i) \tag{3.10}$$

The probability of being in the first intermediate failure region for a given combination of design variables is estimated by a Monte Carlo procedure:

$$P(F_1) \approx \frac{1}{N} \sum_{j=1}^{N} I_{F_1}(\mathbf{x}_j) \tag{3.11}$$

where I_{F_1} is an indicator function, where $I_{F_1}(\mathbf{x}_j) = 1$ if $\mathbf{x}_j \in F_1$ and $I_F(\mathbf{x}_j) = 0$ otherwise. $\mathbf{x}_j$ is the independent and identically distributed samples from the probability density function, f.

The original problem of calculating a small failure probability is that it is computationally demanding. With a proper choice of the intermediate failure

events this can be reduced to calculating a sequence of conditional probabilities with relatively small number of samples. To generate samples from the conditional intermediate failure regions a special Monte Carlo Markov Chain procedure based on the Metropolis algorithm is implemented.

3.5.2 Markov Chain Monte Carlo

Markov Chain Monte Carlo (MCMC) is a method for sampling the distribution of interest, and is based on the concepts of Monte Carlo and Markov Chains techniques (Klüppelberg et al., 2014)

Monte Carlo

Monte Carlo simulation is a numerical simulation method that relies on making repeated calculations with random variables. The outcome of these results will eventually form a basis for a probability distribution. The Monte Carlo simulation is well suited for calculations where several of the input parameters are random variables. The biggest uncertainty will be at the tail of the probability distribution, since it is very unlikely that the minimum or maximum values of all the variables is calculated at the same time.

The classical Monte Carlo method is not efficient in simulating rare events because a large number of samples and model evaluations is required. This can be solved by sampling the distribution of interest by constructing a Markov Chain that has the distribution of interest as its limiting distribution. This is called the Markov Chain Monte Carlo (MCMC) method, and one of the MCMC is the Metropolis-Hastings algorithm, which is modified for sampling the conditional distribution in a way that includes the step where it is checked if the sample points is in the failure region.

Markov Chains

A Markov Chain is a mathematical system that takes in a series of random values, each value being based on the previous value. The characteristic about Markov Chains is that the transition is without memory, meaning that the next state of the process depends only on the current state, and not the previous.

Metropolis-Hastings Algorithm

The main principle behind the Metropolis-Hastings Algorithm is that it generates realizations from a distribution $f(x)$ via proposed distributions, $q(x_0)$, and the acceptance-rejection mechanism defined by a transition kernel. The proposal distribution is a uniform distribution which is centered at the current sample of the chain, x_0, and it is used to generate a proposal sample. A move from the current position of the chain to the proposed sample, x', is accepted with the probability defined by the transition kernel. The chain move if the proposed sample is accepted, otherwise it stays at the same position.

This is how the Metropolis-Hastings Algorithm can control the direction in which the Markov Chain moves. Markov Chain in Metropolis-Hasting algorithm will then converge to the unknown probability distribution of interest under the assumption of ergodicity which will be fulfilled by the reversible transition kernel of the Markov Chain.

3.5.3 Simulated Annealing

Simulated annealing is one of the non-gradient optimization algorithms that can be applied both for continuous and discrete variable spaces. The main difference between this optimization algorithms and other approaches is that it is more sufficient in finding the global minimum, and not only the local minimums. This is because the algorithm allows to escape from local minimums.

The algorithm can be viewed as a continuously attempt to transform the current configurations into one of its neighbors based on randomization techniques (Van Laarhoven and Aarts, 1987). This is done by the Monte Carlo Markov Chain method where a probability density function is used in order to make reasonable guesses in the neighborhood of the initial parameters. If the new random realization leads to an improvement, the properties of the model are update.

The advantage of Simulated Annealing is that it is possible to escape from a local minima and find the global optimum with help of the Metropolis criteria. If the new random guess is an improvement of the original this value is accepted, but if it is not, then the values can still be accepted with a certain probability less than 1. This means that the optimum value also is largely independent of the stating values (Goffe et al., 1994).

Chapter 4

Soil Parameter Estimation based on CPT Data

4.1 Previos Work

Several authors have already discussed how CPT data can be used to estimate parameters and the spatial correlation structures in soil. Some of their work and results are summarized below.

Liu and Chen (2010) estimated spatial correlation structures based on CPT data. The main focus in their research was to estimate the vertical correlation structures and specifically investigate the effects of three factors of interest. These factors where; curve-fitting ranges, equal intervals of measurements and unequal intervals of measurements.

The results from their research indicate that the correlation length of cone tip resistance is more sensitive to different curve-fitting ranges and has larger correlation distance than that of sleeve friction, with respectively mean values of 1.86m and 0.82m. For sampling interval it seems that the mean value of correlation distances is more constant for the equal sampling interval cases than for the unequal cases.

Huber (2013) focused on the evaluation of the effects of soil variability within the framework of probabilistic methods. In one of his case studies, the vertical correlation length was evaluated using CPT databases of different soil types. The results shows that the correlation length of 'sensitive fine grained soils' and 'clean sands to silty sand' is not very different. The subdivision of a soil profile

into layers and the detrending inside each layer on the other hand, has a significant impact on the correlation length

4.2 CPT Data Analysis

The first step in the probabilistic site characterization is to decide preliminary boundaries for different soil layers, and as mentioned above might this have a significant influence on the correlation length estimate. Within each layer, it is assumed that the measurement data fulfil the homogeneity and stationarity criteria. After identifying the layers which tend to be sufficiently homogeneous, these measured data are analyzed to estimate the correlation length, mean value and standard deviation.

If the measured data shows a trend, trend analyses can be conducted by separating the random process into a deterministic trend and a residual variability around the trend. As described in chapter 3, this may reduce the variation of the measured data, but it is important to select this trend with caution. In this study the estimation of soil parameters was based on cone resistance, and no trend was assumed.

4.2.1 Spatial Correlation

The spatial correlation determines how soils are correlated spatially and can be estimated by means of its autocorrelation. The correlation function $\rho(\tau)$ describes how data is correlated with separation distance $\tau = |z_i - z_j|$, which is described in chapter 3. The correlation length, θ, might be dependent on the sample size, and it is recommended to sample with a distance between the measurement points that is at least smaller that 1/5 to 1/4 of the correlation length (Huber, 2013).

4.3 Maximum Likelihood Method

The random field model is implemented to characterize the point and spatial variability of cone resistance from CPT measurements. Maximum likelihood method is an advance estimation technique that is used to describe the random

field parameters. The method estimate the optimal values of correlation length, mean value and standard deviation by maximizing the likelihood function.

The probability of observing a set of data $\mathbf{x}$ is expressed through the likelihood function:

$$L(\mathbf{x}|\mu_x,\sigma_x,\theta) = f_{x_i,...,x_n}(x_1,...,x_n|\mu_x,\sigma_x,\theta) \tag{4.1}$$

which is simply the joint conditional probability density of $x_1,...,x_n$, given assumed values of μ_x, σ_x and θ. If we assume that the data, $\mathbf{x} = \{x_1,...,x_n\}$, are normally distributed, the multivariate normal distribution becomes like the one stated in Eq. 3.3.

Because we assume stationarity in each soil layer, the joint probability function is independent of spatial position and depends only on the relative position of the points. Stationarity also indicates that the mean, covariance and higher order moments are constant in time or space (Fenton and Griffiths, 2008). Hence, this means that the covariance matrix can be written as

$$\mathbf{C} = \sigma_x^2\boldsymbol{\rho} \tag{4.2}$$

where $\boldsymbol{\rho}$ is the correlation matrix

$$\rho_{z_i,z_j} = exp\Big\{-\frac{2}{\theta}|z_i - z_j|\Big\} \tag{4.3}$$

As we see from Eq. 4.3, ρ_{z_i,z_j} is a function of the unknown corelation length, θ. With Eq. 4.2, the likelihood function in Eq. 3.3 can be written as

$$L(\mathbf{x}|\mu_x,\sigma_x,\theta) = \frac{1}{(2\pi\sigma_x^2)^{\frac{n}{2}}|\boldsymbol{\rho}|^{\frac{1}{2}}} \times exp\Big\{-\frac{(\mathbf{x}-\boldsymbol{\mu})^T\boldsymbol{\rho}^{-1}(\mathbf{x}-\boldsymbol{\mu})}{2\sigma_x^2}\Big\} \tag{4.4}$$

$\boldsymbol{\mu}$ is the vector of means corresponding to each observation location. Since we assumed a stationary random field, the mean will be spatially constant and $\boldsymbol{\mu} = \mu_x\mathbf{1}$, where $\mathbf{1}$ is a vector of ones. To find the optimal value of μ_x, σ_x and θ, the likelihood function $L(\mathbf{x}|\mu,\sigma,\theta)$ is maximized. Since the function is strictly nonnegative, maximizing the likelihood function is equivalent to maximizing its logarithm. If we ignore constants, because they will not affect the maximum likelihood estimate, we get:

$$lnL(\mathbf{x}|\mu_x,\sigma_x,\theta) = -\frac{n}{2}ln\sigma_x^2 - \frac{1}{2}ln|\boldsymbol{\rho}| - \frac{(\mathbf{x}-\boldsymbol{\mu})^T\boldsymbol{\rho}^{-1}(\mathbf{x}-\boldsymbol{\mu})}{2\sigma_x^2} \tag{4.5}$$

The maximum of Eq. 4.5 can in principle be found by differentiate with respect to each unknown parameter μ_x, σ_x and θ in turn and setting the results to zero. This will give three equations and three unknown, and the maximum likelihood estimators can be determined (after Fenton and Griffiths, 2008).

$$\mu_x = \frac{\mathbf{1}^T\boldsymbol{\rho}^{-1}\mathbf{x}}{\mathbf{1}^T\boldsymbol{\rho}^{-1}\mathbf{1}} \tag{4.6}$$

$$\sigma_x^2 = \frac{1}{n}(\mathbf{x}-\mu_x\mathbf{1})^T\boldsymbol{\rho}^{-1}(\mathbf{x}-\mu_x\mathbf{1}) \tag{4.7}$$

Eq. 4.6 and 4.7 shows that both the mean and variance estimators can be expressed in terms of the unknown parameter θ. Using this, the maximization problem simplifies to finding the maximum of

$$L(\mathbf{x}|\mu_x,\sigma_x,\theta) = -\frac{n}{2}ln\sigma_x^2 - \frac{1}{2}ln|\boldsymbol{\rho}| \tag{4.8}$$

To calculate the estimate of the correlation length within a layer, the maximum of Eq. 4.8 is found by optimizing the likelihood function versus θ, as shown in Figure 4.1. This maximum value of the likelihood function corresponds to the maximum likelihood estimate of the correlation length, θ.

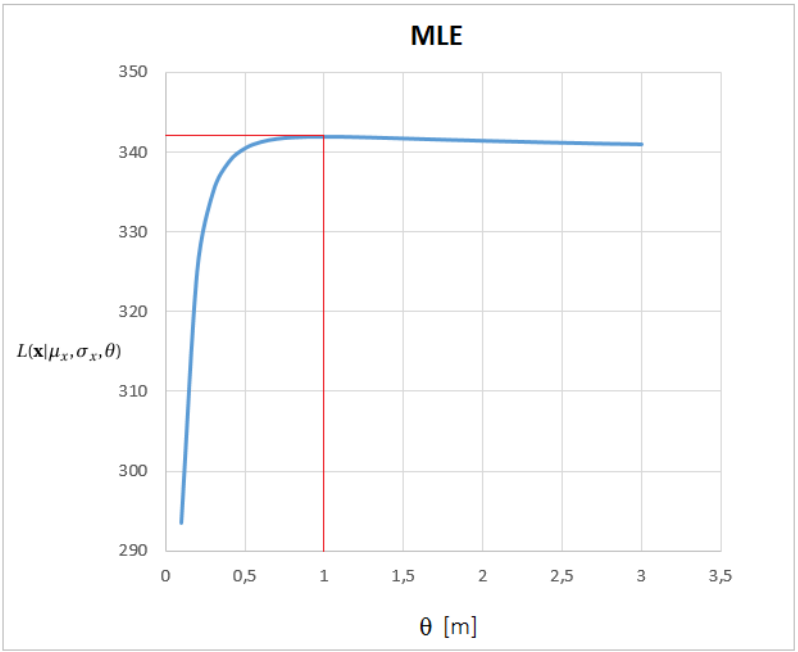

Figure 4.1: Maximum of the likelihood function when $\theta = 1m$

The optimal mean value and standard derivation for this layer can now be estimated by using Eq. 4.6 and 4.7 based on the value for the correlation length which maximizes the likelihood function.

4.4 Soil Parameter Estimation based on CPT Data from Sheringham Shoal wind farm

From CPT measurements the vertical correlation length, mean value and standard deviation of cone resistance from each layer are estimated. These random field parameters are later used for a probabilistic soil parameter interpretation, which is described in chapter 5.

Bolders Bank Formation

18 CPT profiles from Bolders Bank Formation (BDK) were selected for further evaluation, and Table 4.1 shows that the correlation length estimates range between 0.4 and 2.9 m for this soil layer. Figure 4.2 shows the corrected tip resis-

tance, q_t, versus depth for three different boreholes with correlation lengths of 0.4, 1.3 and 2.9. The length of the layer used for determination from each CPT profile can be found in Appendix B.

Table 4.1: Estimated correlation length, mean value and standard deviation BDK

CPT profile	θ [m]	μ_{q_t} [MPa]	σ_{q_t} [MPa]
A3	0.4	1.68	0.39
A4	1.0	2.08	0.60
B1	2.1	1.50	0.70
B2	0.5	1.86	0.45
C1	1.3	1.87	0.44
C2	0.8	1.79	0.61
C4	2.4	1.94	0.55
C7	2.4	2.00	0.65
D3	1.7	1.91	0.61
D4	2.3	1.62	0.78
E1	0.4	1.83	0.34
H5	2.9	2.22	0.88
I1	1.2	2.39	0.84
I4	1.6	2.52	0.84
I6	0.8	1.97	0.46
J2	1.7	2.22	0.79
J6	1.2	1.81	0.55
K2	0.6	1.95	0.63
mean values	1.5	1.89	0.60

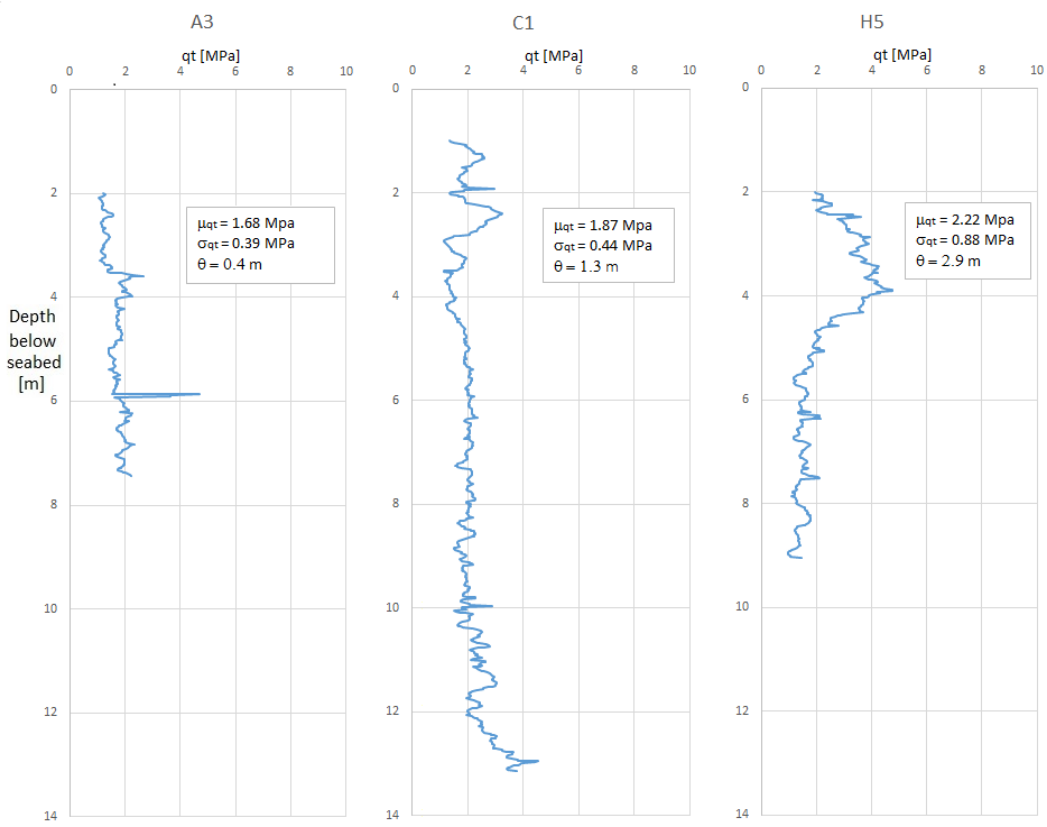

Figure 4.2: Corrected tip resistance versus depth for three different CPT profiles, all with different correlation lengths

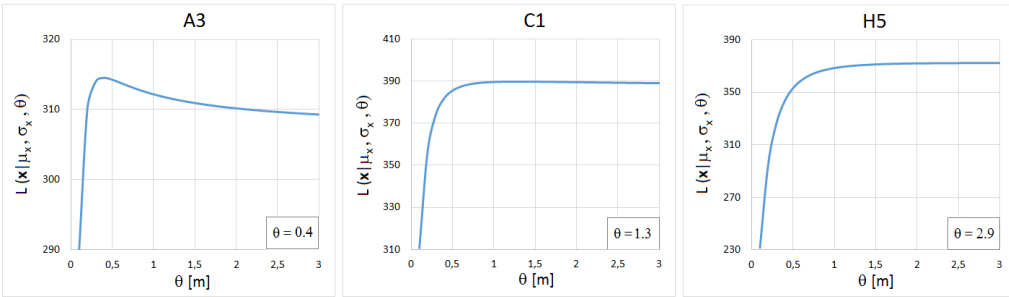

Figure 4.3: Maximum likelihood function plotted against correlation length for three different CPT profiles

Figure 4.2 shows how the corrected cone tip resistance is varying with depth for three different borehole locations, and Figure 4.3 shows the three corresponding plots of the maximum likelihood function. Different lengths of the layer used for interpretation may effect the estimated value of the vertical correlation length. If the CPT measurements from 2 - 5 m is removed from profile H5, a correlation length of 0.5 m is estimated. The likelihood function of profile C1 and H5 also indicates that the value of the function is almost the same from around θ = 0.7 m to θ = 3 m .

Swarte Bank Formation

11 CPT profiles from Swarte Bank Formation (SBK) were selected for further evaluation. Table 4.2 shows that the correlation length estimates range between 0.5 and 3.0 m, which is similar to the estimated values from BDK. The length of the layer used for determination from each CPT profile can be found in Appendix B.

Table 4.2: Estimated correlation length, mean value and standard deviation SBK

CPT profile	θ [m]	μ_{q_t} [MPa]	σ_{q_t} [MPa]
A7	2.0	5.98	2.53
C6	3.0	9.75	3.55
D6	0.9	9.57	2.26
E8	0.5	10.38	2.44
F6	1.9	5.99	2.51
G6	3.0	9.46	3.54
H1	1.1	7.02	4.84
I1	2.1	10.79	6.04
I4	1.1	8.79	4.16
I6	1.2	6.81	1.85
J6	1.3	9.84	3.52
mean values	1.6	8.58	3.39

Chapter 5

Probabilistic Soil Parameter Interpretation from CPT Data

5.1 Link Between Soil Parameters and CPT Parameters

CPT measurements provide a basis for interpretation of a wide range of soil parameters for both strength and deformation. Due to uncertainties associated with CPT measurements and the soil parameter interpretation it is of interest to conduct a probabilistic CPT interpretation.

For a reliability-based design of a monopile foundation, where the soil conditions at the pile penetration depth mainly consists of clay and sand layers, interpretation of undrained shear strength and friction angle are of high interest.

5.2 Interpretation of Undrained Shear Strength based on CPT Data

To determine the soil resistance for clay under fully plastic behaviour, which is used when modelling p-y curves, the undrained shear strength, S_u, is an important parameter. S_u is directly related to the peak value of soil resistance, and variability of S_u is expected to have a significantly influence on the pile-soil responce.

The undrained shear strength of clay is not a unique parameter and no sin-

gle undrained shear strength exists. The parameter depends significantly on the orientation of the failure planes, the type of test used, soil anisotropy, rate of strain and stress history.

Equation 5.1 shows the empirical approach available for interpretation of S_u from CPT/CPTU using corrected cone tip resistance. This approach can also be denoted as a transformation model that is needed to relate the test measurement to an appropriate design property (Phoon and Kulhawy, 1999). The design parameter in this case is the undrained shear strength. To use this parameter in a reliability-based design uncertainties related to the transformation model are evaluated.

$$s_u = \frac{(q_t - \sigma_{v0})}{N_k} \tag{5.1}$$

where:
q_t =corrected cone tip resistance [MPa]
σ_{v0} =in situ overburden pressure [kPa]
N_k =empirical cone factor

5.2.1 Corrected Cone Tip Resistance

If the values of corrected cone resistance, q_t, is plotted in a histogram as shown in Figure 5.1, it might be reasonable to assume that q_t is log-normally distributed. This indicates that ln_{q_t} is normally distributed, and the multivariate normal distribution of the ln_{q_t} random field becomes like the one stated in Eq. 3.3.

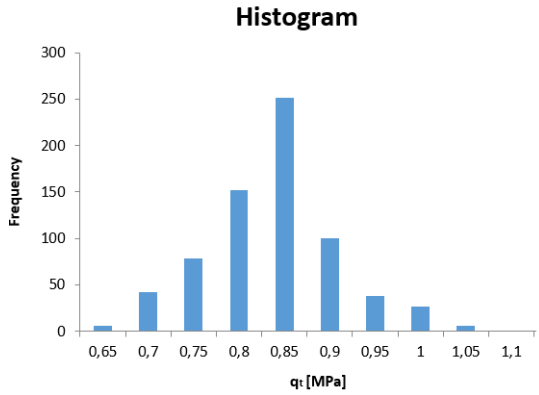

Figure 5.1: Histogram showing the distribution of corrected tip resistance

By using the maximum likelihood method, as described in chapter 4, we can determine the correlation length, mean value and standard deviation for the $\ln q_t$ random field.

When we have calculated μ_{lnq_t} and σ_{lnq_t}, we can find the corresponding normal distribudet parameters by Eq. 5.2 and 5.3.

$$\mu_{q_t} = exp\left(\mu_{lnq_t} + \frac{\sigma^2_{lnq_t}}{2}\right) \tag{5.2}$$

$$\sigma_{q_t} = \mu_{q_t}\sqrt{exp(\sigma^2_{lnq_t}) - 1} \tag{5.3}$$

5.2.2 Empirical Cone Factor

N_k is generally obtained from empirical correlations , and should not be a constant value that is valid for all clays (Robertson and Campanella, 1983a). Previous research (e.g Aas et al. (1986), Lunne et al. (1976) and Rad and Lunne (1989)) shows that the value might depend on factors like over consolidation ratio, plasticity index and the reference test that has been used. For undrained shear strength NGI favor the use of results from consolidated anisotropically triaxial compression tests (CAUC) to develop consistent correlation from CPTU data (Karlsrud et al., 1997).

If we want to establish a probabilistic link between undrained shear strength and CPT data we need to consider the uncertainty in the empirical cone factor. Kulhawy et al. (1992) developed a database for sites in clay to determine the

correlation between measured CPTU and undrained shear strength determined from consolidated isotropic undrained triaxial compression (CIUC), unconsolidated undrained triaxial compression (UU) and vane shear test (VST). The coefficient of variation (CoV) for N_k was found to bee between 29-40%, dependent on test used to determine the undrained shear strength. For CIUC triaxial test the CoV of N_k was around 35%.

In this case ,soil from Sheringham Shoal wind farm is considered. From the Bolders Bank Formation and the Swarte Bank Formation a cone factor of N_k=15 provides reasonable correlation with the available laboratory test data (Saue and Meyer, 2009). For the static shear strength this value was evaluated based on CAUC tests. This value is selected as the mean value and the CoV evaluated from CIUC is assumed. Based on eq. 5.4 the standard deviation for the empirical cone factor will be $\sigma_{N_k} = 5.25$. This might seem like a high standard deviation for a cone factor, but due to the limited available information this value is assumed.

$$CoV_{N_k} = \frac{\sigma_{N_k}}{\mu_{N_k}} \tag{5.4}$$

From equation 5.1 wee see that N_k equal to zero or a negative value will not give a physically meaningful value of S_u, and a log-normally distribution of N_k is assumed. We use eq. 5.5 and 5.6 to find the corresponding parameters for the lognormal distribution.

$$\mu_{lnN_k} = ln\left(\frac{\mu_{N_k}}{\sqrt{1+\frac{\sigma^2_{N_k}}{\mu^2_{N_k}}}}\right) \tag{5.5}$$

$$\sigma_{lnN_k} = \sqrt{ln\left(1+\frac{\sigma^2_{N_k}}{\mu^2_{N_k}}\right)} \tag{5.6}$$

5.2.3 Undrained Shear Strength

Now that we have determined a distribution for both the corrected cone tip resistance and the cone factor, these can be used to determine the log-normally distributed parameters of $\ln S_u$ where:

$$lnS_u = ln(q_t - \sigma_{v0}) - lnN_k \tag{5.7}$$

$$\mu_{lnS_u} = \mu_{ln(q_t-\sigma_{v0})} - \mu_{lnN_k} \tag{5.8}$$

$$\sigma_{lnS_u} = \sqrt{\left(\frac{\partial lnS_u}{\partial ln(q_t-\sigma_{v0})}\sigma_{ln(q_t-\sigma)}\right)^2 + \left(\frac{\partial lnS_u}{\partial lnN_k}\sigma_{lnN_k}\right)^2} = \sqrt{\sigma^2_{ln(q_t-\sigma_{v0})} + \sigma^2_{lnN_k}} \tag{5.9}$$

The overburden total stress σ_{v0} is assumed to be deterministic, such that

$$\sigma_{v0} = z\gamma + z_w\gamma_w \tag{5.10}$$

Where:
z = depth below seabed [m]
z_w = water depth [m]
γ_w = water density $\left[kN/m^3\right]$

The soil density, γ, is assumed to be constant within each layer and the the total overburden stress will increase linearly with depth. This gives us $\mu_{(q_t-\sigma_{v0})}$ and $\sigma_{(q_t-\sigma_{v0})}$, which is $\mu_{q_t} - \sigma_{v0}$ and σ_{q_t}, respectively. Such as for the cone factor N_k we need to use equation 5.5 and 5.6 to find the log-normally distributed parameters, $\mu_{ln(q_t-\sigma_{v0})}$ and $\sigma_{ln(q_t-\sigma_{v0})}$.

5.2.4 S_u Random Field Generation

To characterize the point and spatial variability of undrained shear strength, a random field model is utilized.

When determining the correlation length, mean value and standard deviation from q_t, we assumed stationarity within the layer. Since μ_{lnS_u} and σ_{lnS_u} is dependent on the total overburden pressure, these will vary linearly with depth and the layer does no longer fulfil the requirements of being stationary. $\boldsymbol{\mu}_{lnS_u}$ and $\boldsymbol{\sigma}_{lnS_u}$ will be vectors and can be written as:

$$\boldsymbol{\mu}_{lnS_u} = \alpha_1 + \alpha_2 \times \mathbf{z} \tag{5.11}$$

$$\boldsymbol{\beta}_{lnS_u} = \beta_1 + \beta_2 \times \mathbf{z} \tag{5.12}$$

Where α_1, α_2, β_1 and β_2 are the linear trend parameters and z is depth below seabed. Figure 5.3 and 5.4 show an example of mean value and standard deviation of the lognormally distributed parameters of S_u varying with depth. As seen in Figure 5.3, μ_{lnSu} is decreasing with depth. Figure 5.2 shows recorded values of q_t versus depth. Due to a constant μ_{q_t}, the mean value of S_u will decrease with depth.

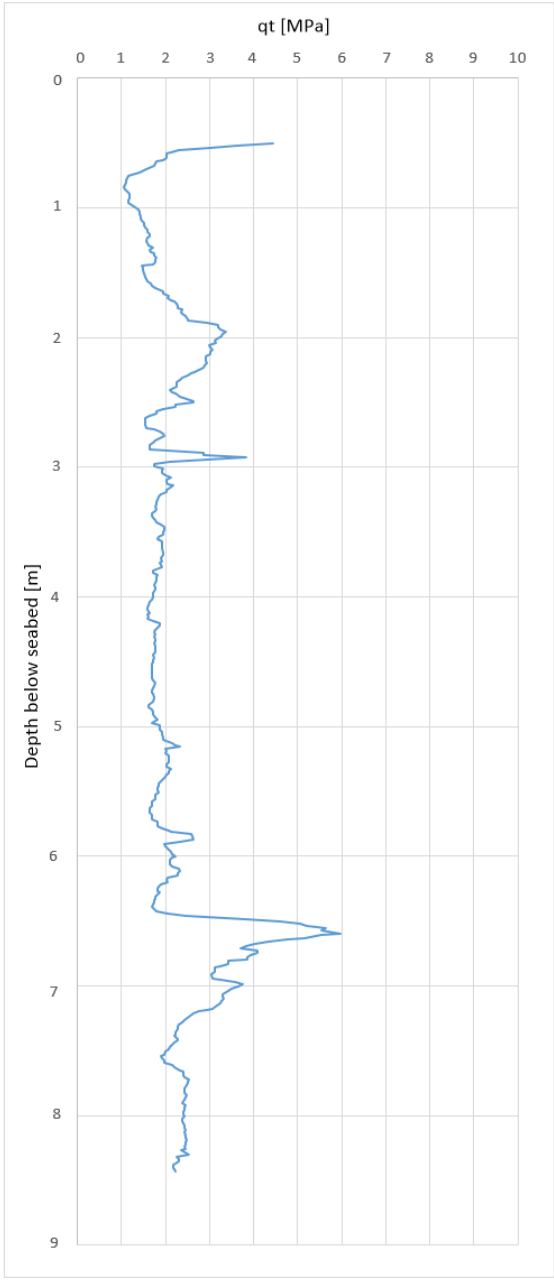

Figure 5.2: CPT measurement from Sheringham Shoal wind farm showing recorded values of q_t versus depth

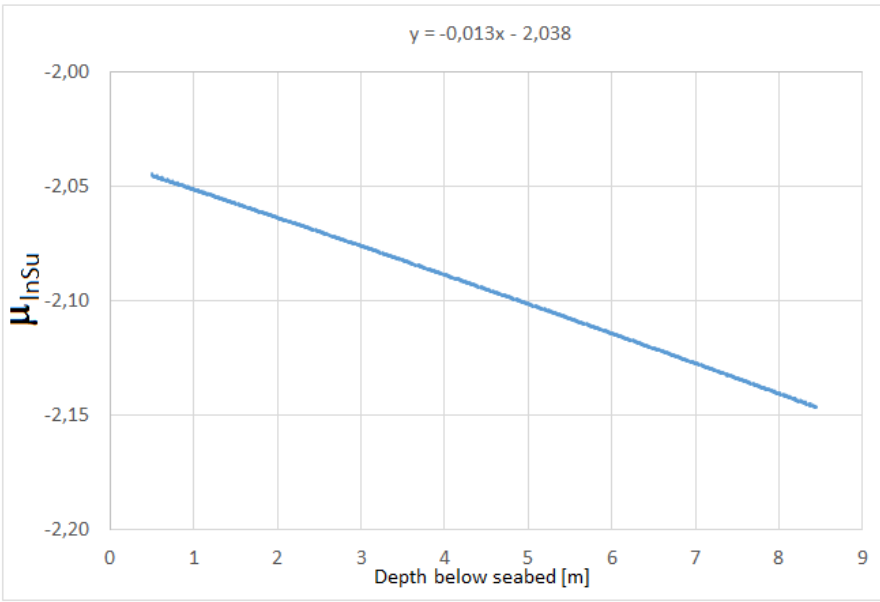

Figure 5.3: Mean value of $\ln S_u$ with depth, with $\alpha_1 = -2,0$ and $\alpha_2 = -0,013$

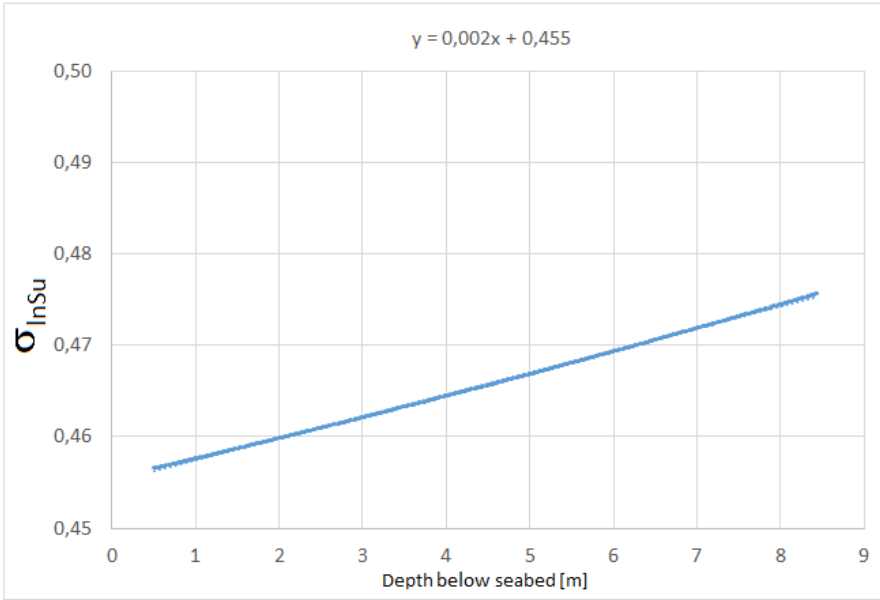

Figure 5.4: Standard deviation of $\ln S_u$ with depth, with $\beta_1 = 0,46$ and $\beta_2 = 0,002$

Because σ_{lnS_u} is dependent with depth, the covariance matrix, **C**, will also be depend on the standard deviation between two points of the random field discretization:

$$\mathbf{C} = \begin{bmatrix} \sigma_{z_1}^2 & \sigma_{z_1}\sigma_{z_2}\rho(z_1,z_2) & .. & \sigma_{z_1}\sigma_{z_n}\rho(z_1,z_n) \\ \sigma_{z_2}\sigma_{z_1}\rho(z_2,z_1) & \sigma_{z_2}^2 & .. & \sigma_{z_2}\sigma_{z_n}\rho(z_2,z_n) \\ : & : & & : \\ : & : & & : \\ \sigma_{z_n}\sigma_{z_1}\rho(z_n,z_1) & \sigma_{z_n}\sigma_{z_2}\rho(z_n,z_2) & .. & \sigma_{z_n}^2 \end{bmatrix} \tag{5.13}$$

To generate a random field realization of S_u, we need to perform a Cholesky decomposition of the covariance matrix:

$$\mathbf{C} = \mathbf{A}\mathbf{A}^T \tag{5.14}$$

where **A** is the lower triangular. The random field realization of the undrained shear strength can now be determined by Eq. 5.15, and Figure 5.5 shows an example of a random field of S_u based on the values for $\boldsymbol{\mu}_{lnS_u}$ and $\boldsymbol{\sigma}_{lnS_u}$ as given in Figure 5.3 and 5.4.

$$S_u = exp \times (\boldsymbol{\mu}_{lnS_u} + \mathbf{A}\mathbf{T}) \tag{5.15}$$

where **T** is a vector of standard normal distributed random variables with mean value 0 and standard deviation 1, $\mathbf{T} \sim N(0,1)$.

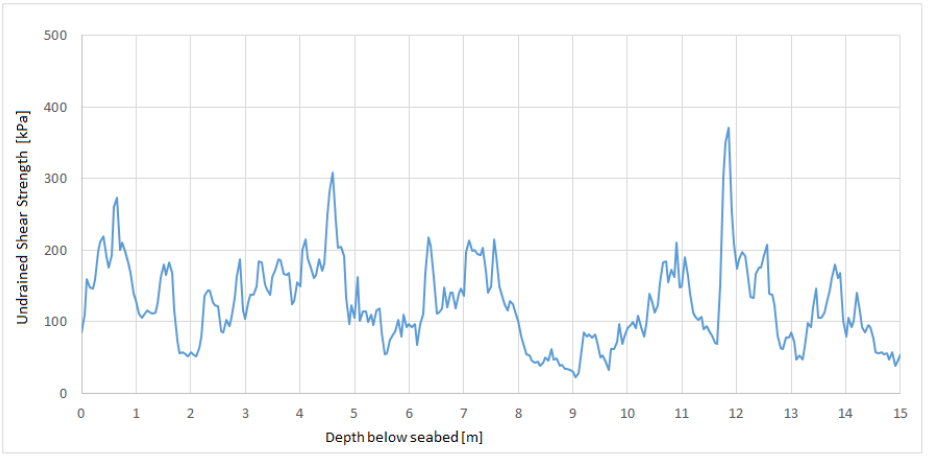

Figure 5.5: Random field of undrained shear strength with correlation length θ=1 m

5.3 Interpretation of Friction Angle based on CPT Data

For construction of p-y curves for sand the variability of friction angle, φ, is expected to significantly influence the pile-soil response. The ultimate soil resistance for sand is calculated by dimensionless coefficients which depends on φ.

Robertson and Campanella (1983b) reviewed calibration chamber test results to compare measured cone penetration resistance, q_c, to measured friction angle from drained compression triaxial tests (also cited by Lunne et al., 1997). These triaxial tests were performed at confining stresses approximately equal to the horizontal effective stress in the calibration chamber before cone penetrating.

Robertson and Campanella (1983b) proposed an average correlation and developed a useful design chart for estimation of friction angle from cone penetration resistance, as shown in Figure 5.6. It can be expected that this chart will provide resonable estimates of friction angle for sands similar to those used in the chamber studies. This was moderately imcompressible, normally consolidated and predominantly quartz sands. For highly compressible sands the chart would tend to predict conservatively low friction angles.

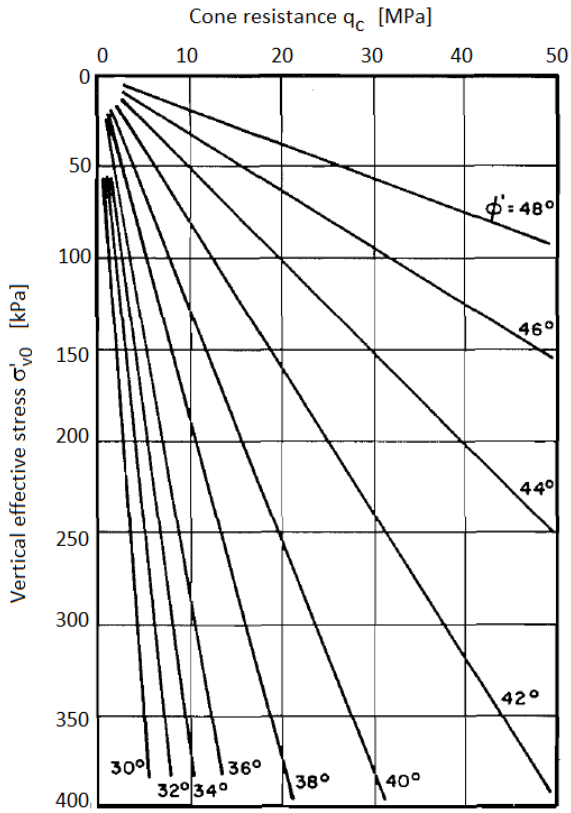

Figure 5.6: Relationships between φ', q_c and σ'_{v0} (after Robertson and Campanella, 1983b)

Figure 5.6 shows that q_c is linearly increasing with σ'_{v0} for constant φ'. To use this chart for further interpretation of the friction angle based on CPT data from Sheringham Shoal, the transformation must be expressed by a corresponding function. The first step would be to express the ratio between q_c and σ'_{v0}, here denoted as β:

$$\beta = \frac{q_c}{\sigma'_{v0}} \tag{5.16}$$

Where:
q_c = Cone resistance [MPa]
σ'_{v0} = Vertical effective stress [kPa]

Each value of β gives a value of φ', as shown in Figure 5.7. By adding a trendline

between theses values an expression of φ' is given, which is based on the ratio between q_c and σ'_{v0}. This relation can be expressed by Eq. 5.17, where ε is the transformation uncertainty. This equation is also very similar to the interpretation equation between triaxial compression effective stress friction angle and the cone tip resistance described by Kulhawy and Mayne (1990).

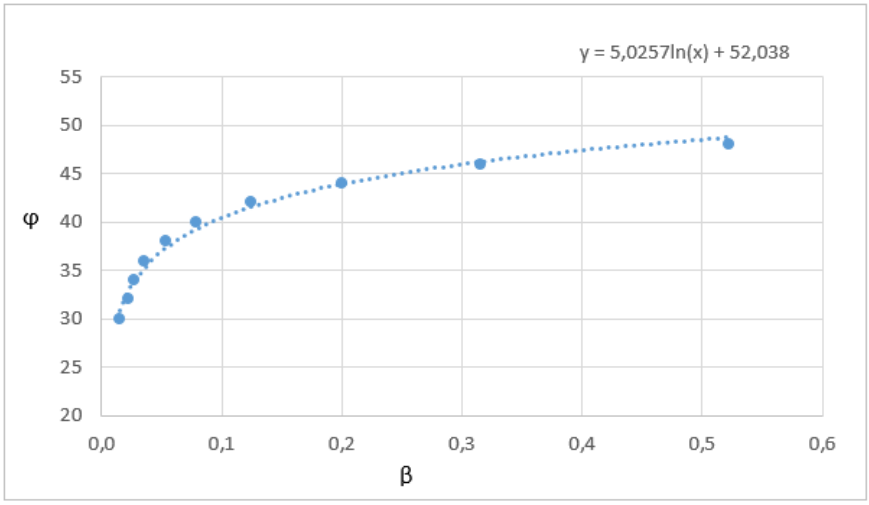

Figure 5.7: Determination of φ' based on the ratio between q_c and σ'_{v0}, denoted as β

$$\varphi(\beta) = 5.03ln(\beta) + 52.04 + \varepsilon \tag{5.17}$$

5.3.1 Cone Tip Resistance

Similarly as for clay, the cone tip resistance, q_c, in a sand layer is assumed to be lognormally distributed. The cone tip resistance will be spatially correlated, and it is of interested o find the parameters that describes the random field model. This is done by the same method as for the corrected cone tip resistance, and we can estimate θ, μ_{lnq_c} and σ_{lnq_c} for the $\ln q_c$ random field. Figure 5.8 shows recorded values of q_c, and it might be reasonable to assume that μ_{q_c} and σ_{q_c} are not dependent on position.

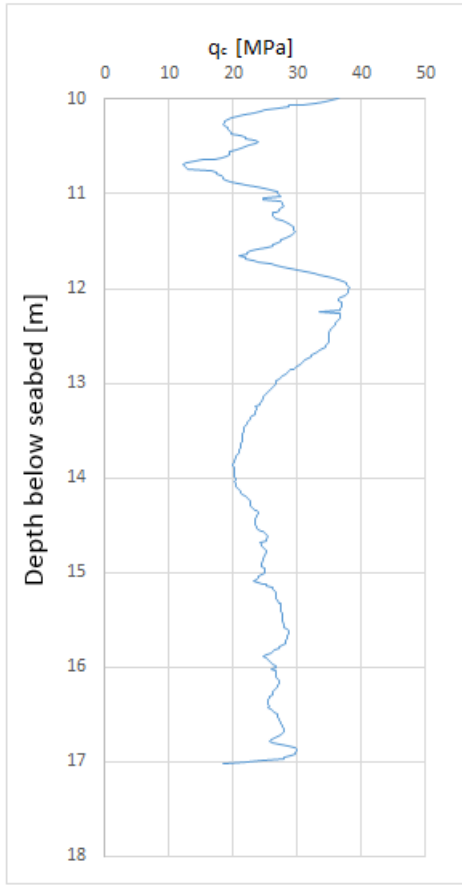

Figure 5.8: CPT measurement from Sheringham Shoal wind farm showing recorded values of q_c versus depth for Egmond Ground Formation

5.3.2 Generate a Random Field Realization of Friction Angle

To determine the mean value and standard deviation for the φ random field we use Eq. 5.18 and 5.19.

$$\mu_\varphi = 5.03\mu_{lnq_c} - 5.03ln(\sigma'_{v0}) + 52.04 + \mu_\varepsilon \tag{5.18}$$

$$\sigma^2_\varphi = (5.03\sigma_{lnq_c})^2 + \sigma^2_\varepsilon \tag{5.19}$$

The vertical effective stress σ'_{v0} is assumed to be deterministic, such that

$$\sigma'_{v0} = z\gamma' \tag{5.20}$$

where z is depth below seabed and γ' is effective soil density, which is assumed to be constant within each layer, and the effective stress will hence increase linearly with depth. The mean value of the transformation uncertainty, μ_ε, is zero and the standard deviation, σ_ε, for this interpretation is 2.8° (Kulhawy and Mayne, 1990). Figure 5.9 shows an exaple of a random field of φ.

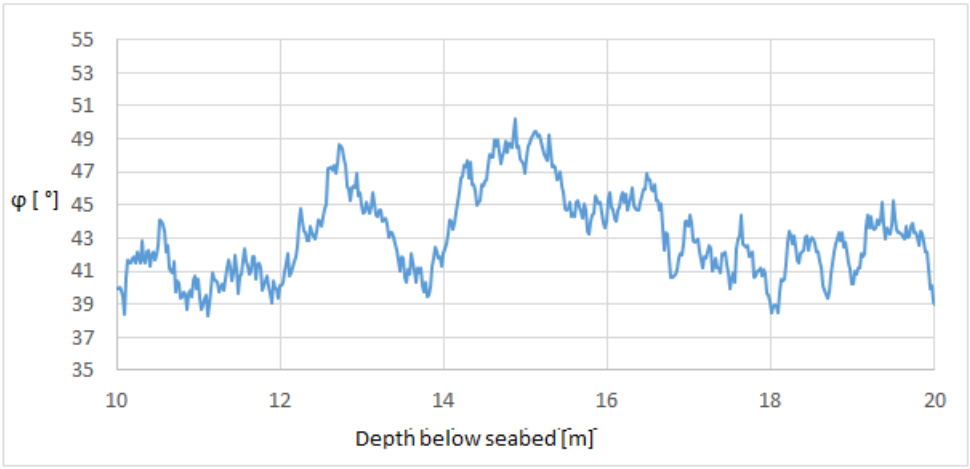

Figure 5.9: Random field of friction angle with correlation length θ=1.5 m

5.4 CPT Parameter Interpretation and the P-Y Model

After the probabilistic models for S_u and φ are constructed, they are utilized in the reliability analysis of monopile foundation. The pile penetration length, L_p, is discretized in P equal intervals, with interval length of $dl = \frac{L_p}{P}$. As stated earlier the soil response is simulated by a series of independent springs with material behavior defined by p-y curves. Each spring is represent by a p-y curve, which is calculated based on the soil type and depth at this point.

Figure 5.10 shows how the total pile penetration length, L_p is subdivided into three layers, where z_1 is the boundary between Bolders Bank and Edmond Ground Formation, z_2 is the boundary between Egmond Ground and Swarte Bank Foundation and z_3 is set to 40 m, which is set as the maximum length

of penetration in the RBDO. Two CPT profiles from Sheringham Shoal were selected and the layer boundaries for these profile are summarized in Table 5.1

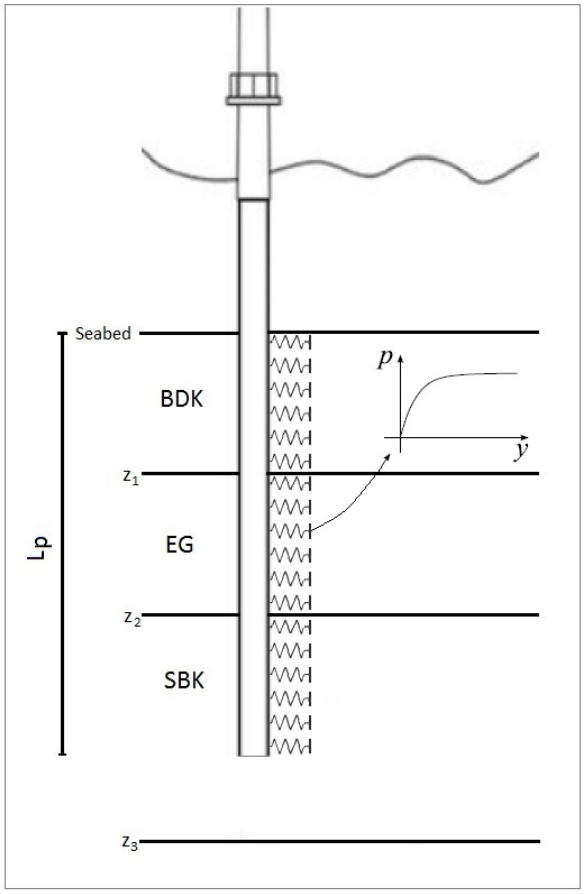

Figure 5.10: Pile penetration length, L_p, subdivided into three different layers which will have different parameters for their random field determination

Table 5.1: Layer boundaries

CPT profile	Water depth [m]	z_1 [m]	z_2 [m]	z_3 [m]
I1	18	10	18	40
I4	18	10	15	40

BDK and SBK are characterized as stiff clay. The p-y curves from these layers are constructed after the method proposed by Reese et al. (1975). S_u is directly related to the ultimate soil resistance, p_u, and the parameters for generating S_u random fields are needed. EG is characterized as a sand layer, and the p-y curves for this layer are constructed after the modified expression suggested by O'Neill and Murchison (1983). As stated earlier, p_u for sand depends on the value of φ, and the parameters for generating φ random fields are needed. The probabilistic soil parameters of S_u and φ from CPT profile I1 and I4 are summarized in Table 5.2 and 5.3.

Table 5.2: Random field parameters for I1

	θ [m]	α_1	α_2	β_1	β_2
BDK	1.2	-1.9	-1.2×10^{-2}	0.50	2.7×10^{-3}
EG	1.5	48	-0.38	2.99	0
SBK	2.1	-0.43	-2.7×10^{-3}	0.63	8.6×10^{-4}

Table 5.3: Random field parameters for I4

	θ [m]	α_1	α_2	β_1	β_2
BDK	1.6	-1.9	-1.1×10^{-2}	0.49	2.4×10^{-3}
EG	3.0	49	-0.39	3.65	0
SBK	1.1	-0.6	-3.1×10^{-3}	0.56	8.9×10^{-4}

Chapter 6

Results

6.1 Reliability-based Design Optimization of a Monopile Foundation

6.1.1 Problem Definition

The goal of RBDO is to find the monopile design parameters, **t**=[D, w, L_p], which minimize the cost and provide a safe design at the same time. In this study, the design cost is defined to be proportional to the monopile weight and failure probability:

$$C(\mathbf{x},\mathbf{t}) = C_i(\mathbf{t})L_p\rho_s\pi\left[\left(\frac{D}{2}\right)^2 - \left(\frac{D}{2}-w\right)^2\right] + C_F P_F(\mathbf{x},\mathbf{t}) \tag{6.1}$$

Where:
L_p = pile embedded length [m]
ρ_s = density of steel [kN/m^3]
D = pile diameter [m]
w = pile wall thickness [m]

$C_i(\mathbf{t})$ is the cost of production and installation which is assumed to be 2 €/kg of the monopile, C_F is the failure cost and is estimated to be 10^7 €. P_F(**x,t**) is the probability of failure, which defines the probability of exceeding the ultimate limit state.

The reliability analysis is performed by evaluating the effects of variability in

undrained shear strength of clay, friction angle of sand and lateral load. The random fields of S_u and φ are used in the pile-soil system to determine p-y curves of stiff clay and sand, where the distance between each uncoupled spring is 1 m . Other parameters used in calculations of p-y curves are assumed to be deterministic. These parameters and their values are summarized in Table 6.1.

Table 6.1: Parameters used for p-y curves

Symbol	Explanation	Value	Unit
J	Empirical model parameter	0.25	-
γ'	Submerged unit weight	18	kN/m^3
ε_{50}	Strain at one-half the ultimate soil resistance	0.005	-

Random Load

The characteristic for an offshore wind turbine is that the support structure is subjected to dominant lateral loading due to wind and wave loading. In this study the force resulting from wind and wave loading is approximated by a horizontal force. For a modern offshore wind turbine, located in 20 m water depth, it is assumed that this force will act approximately 30 m above seabed level (LeBlanc, 2009). This consequently results in a moment $M = H \times m$ applied at the sea bed level.

The uncertainties in the load are assumed to be distributed according to the Gumbel distribution whit a mean value $\mu_H = 2500$ kN. According to Agarwal and Manuel (2009) is it reasonable to assume a coefficient of variation of $CoV_H = 0.2$.

Design parameters

The reliability analysis is conducted to optimize the cost of the foundation with respect to the monopile diameter, D, the wall thickness, w, and the embedded pile length, L_p. Optimization is conducted in the discretized domain, Ω_t, such that $D \in [4.0, 4.1, ..., 7.0]$, $w \in [0.03, 0.04, ..., 0.10]$ and $L_p \in [25, 26, ..., 40]$:

$$[4, 0.03, 25]^T \leq \mathbf{t} \leq [7, 0.1, 40]^T \tag{6.2}$$

Parameter for the steel pile is the density of steel, $\rho_s = 7850$ kN/m^3, Young's modolus of steel pile, $E_p = 2.1 \times 10^5$ MPa and Poisson's ratio of steel, $v_s = 0.3$.

6.1.2 Ultimate Limit State

The reliability-based design optimization is performed by considering the uncertainties in $\mathbf{U} = [S_u, \varphi, H]^T$ on the ultimate limit state for the monopile. The ultimate limit state in this study is defined by the steel yield stress, $\sigma_{lim} = 235$ MPa. The performance function for the ultimate limit state is defined as:

$$g(\hat{\mathbf{x}},\hat{\mathbf{t}}) = \sigma_{lim} - \sigma(\hat{\mathbf{x}},\hat{\mathbf{t}}) \tag{6.3}$$

where $\sigma(\hat{\mathbf{x}},\hat{\mathbf{t}})$ is the maximum stress in the monopile for a given combination of $\hat{\mathbf{x}}$ and $\hat{\mathbf{t}}$.

6.1.3 Subset Simulation

Based on a given combination of design variables, $\hat{\mathbf{t}}$, we want to find the probability of failure, $P_F(\mathbf{x},\hat{\mathbf{t}})$. Subset simulation method has an efficient and robust performance when small P_F is to be evaluated, and is in this study used to find $P_F(\mathbf{x},\hat{\mathbf{t}})$:

$$P_F(\mathbf{x},\hat{\mathbf{t}}) = P(F_1\mathbf{x},\hat{\mathbf{t}}) \prod_{i=1}^{k-1} P(F_{i+1}(\mathbf{x},\hat{\mathbf{t}})|F_i(\mathbf{x},\hat{\mathbf{t}}) \tag{6.4}$$

where the conditional failure probability is set to P=0.1.

The reliability limit of the structure is specified as P_F^{lim}. For offshore wind turbines the value of $P_F^{lim} = 10^{-4}$ is selected based on the analysis of the failure consequences associated with exceeding the ultimate limit state (Sorensen and Tarp-Johansen, 2005). To satisfy the reliability constraint, $P_F(\mathbf{x},\hat{\mathbf{t}}) \leq P_F^{lim} = 10^{-4}$, the cost of the monopile is set to $C(\mathbf{x},\hat{\mathbf{t}}) = \infty$ in the case when $P_F(\mathbf{x},\hat{\mathbf{t}}) > 10^{-4}$.

6.1.4 Simulated Annealing

The Simulated Annealing (SA) algorithm is in this study used to search for the minimum of Eq. 6.1 and account for the reliability limit of the structure at the same time.

The initial value of the design parameters in the SA algorithm is set to $\mathbf{t}^{(1)} = [5.5, 0.05, 30]$, with $P_F(\mathbf{x},\hat{\mathbf{t}}) < 10^{-6}$ and $C(\mathbf{x},\hat{\mathbf{t}}) = 4.03 \times 10^5$ €.

Simulations of the Simulated Annealing algorithm were conducted with uniform proposal distributions where the current state of design parameters, $\hat{\mathbf{t}}$, is

the center of the distribution. The uniform proposal distribution will then be distributed with limits $\pm\mathbf{h}$ such that U($\hat{\mathbf{t}}$-$\mathbf{h}$, $\hat{\mathbf{t}}$+$\mathbf{h}$) with $\mathbf{h} = [0.1, 0.01, 1]$.

6.2 Summary of Results

Correlation lengths, random field realizations and optimal design parameters were calculated for two different borehole locations at the wind farm site. The result from these calculations are used as input parameters in the RBDO. Table 5.2 and 5.3 shows the random field parameters, which are used for integration with p-y curves.

6.2.1 CPT Profile I1

As we see from Table 5.1 the water depth at this location is 18 m , Bolders Bank formation is 0-10 m below seabed, Egmond Ground 10-18 m and Swarte Bank from 18 m below seabed and down to the optimal penetration length of the monopile. The calculated correlation lengths from each layer is shown in Figure 6.1, and Figure 6.2 shows examples of random field realizations from this location, one for each layer.

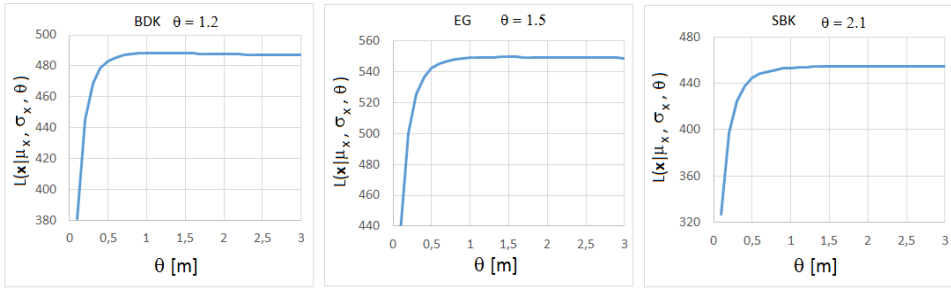

Figure 6.1: Makimum likelihood estimates of correlation length for layers at CPT profile I1

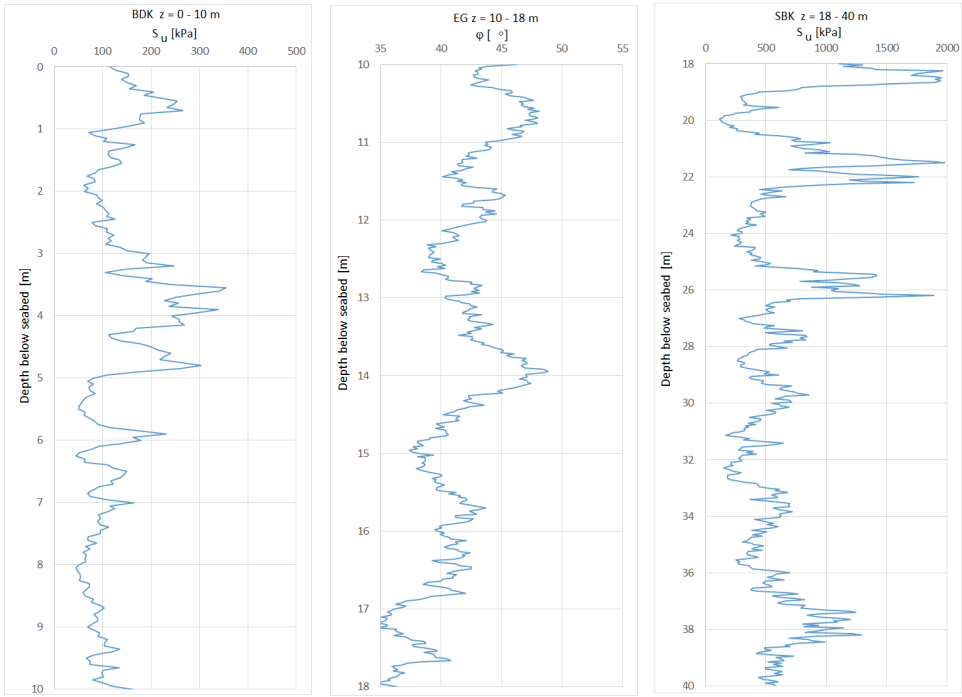

Figure 6.2: Random field realizations for CPT profile I1

Simulated Annealing

Seven calculations for CPT profile I1 were performed with the Simulated Annealing stochastic optimization algorithm. The algorithm was coupled with the Subset Simulation (SS) to estimate the failure probabilities. Simulations of the algorithm with 1000 iterations were performed. Subset Simulation algorithm was performed with 200 simulations per step. Figure 6.3-6.7 shows the calculated values of costs, pile embedded length, pile wall thickness, pile diameter and probability of failure of the first three calculations. Table 6.2 shows the minimum costs and related parameters from each calculation.

Table 6.2: Optimal minimum costs for CPT profile I1 based on SA Optimization

N_s	Calculation number [-]	$C(\mathbf{x},\mathbf{t})$ [€]	L_p [m]	w [m]	D [m]	P_F [-]
200	1	$2.55x10^5$	26	0.04	5	8.5×10^{-6}
200	2	$2.60x10^5$	26	0.04	5.1	4.6×10^{-6}
200	3	$2.64x10^5$	27	0.04	5	8.5×10^{-6}
200	4	$2.90x10^5$	27	0.04	5.7	3.3×10^{-6}
200	5	$2.70x10^5$	27	0.04	5.1	8.5×10^{-6}
200	6	$2.65x10^5$	26	0.04	5.2	7.9×10^{-5}
200	7	$2.75x10^5$	26	0.04	5.4	3.9×10^{-5}

Table 6.2 shows that the optimal design cost for these calculations is varying between $2.55 - 2.90x10^5$ €. The optimal pile wall thickness is consistently 0.04 m , L_p is 26 m or 27 m and D is varying between 5-5.7 m. Figure 6.7 shows that the SA algorithm satisfies the reliability constraint since $P_F \leq P_F^{lim}$ for all the proposed design parameters.

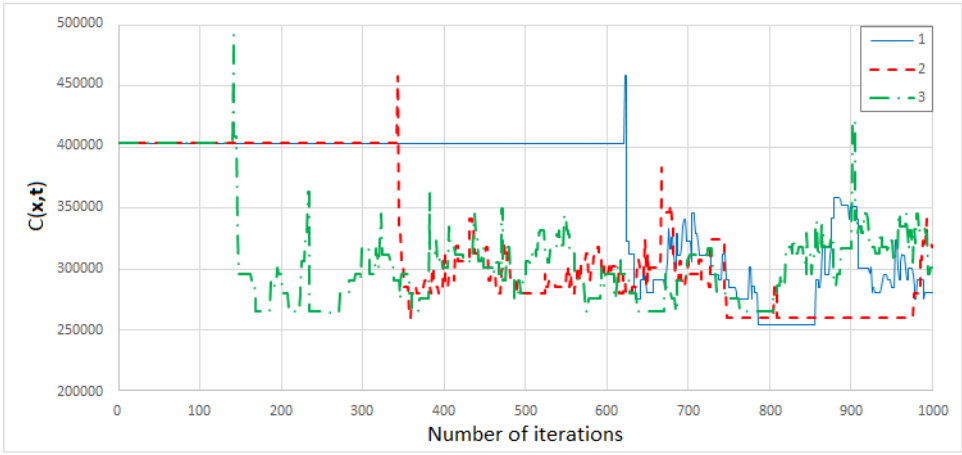

Figure 6.3: SA optimization I1 - Design cost of the monopile, C(**u,t**), from three different calculations

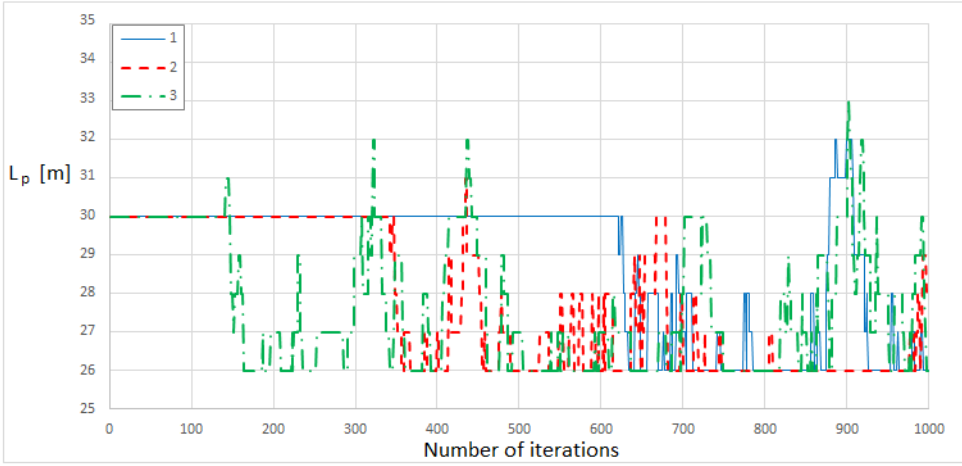

Figure 6.4: SA optimization I1 - Pile embedded length, L_p, from three different calculations

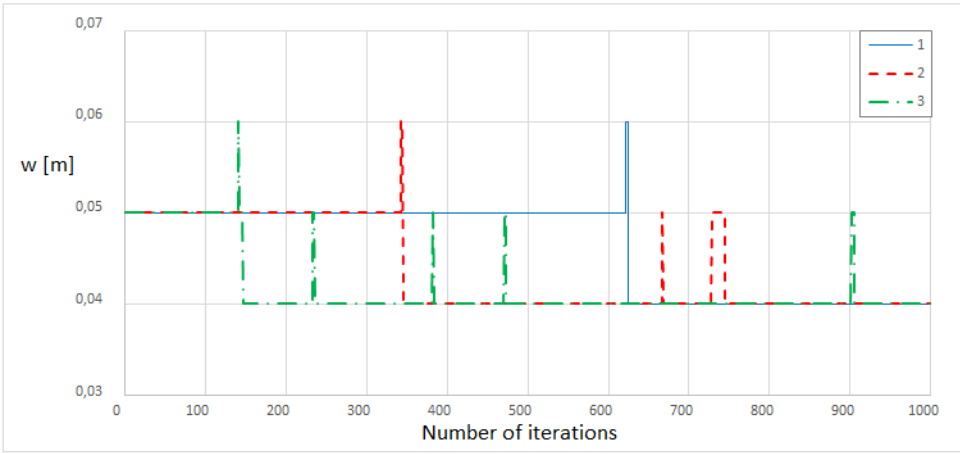

Figure 6.5: SA optimization I1 - Pile wall thickness, w, from three different calculations

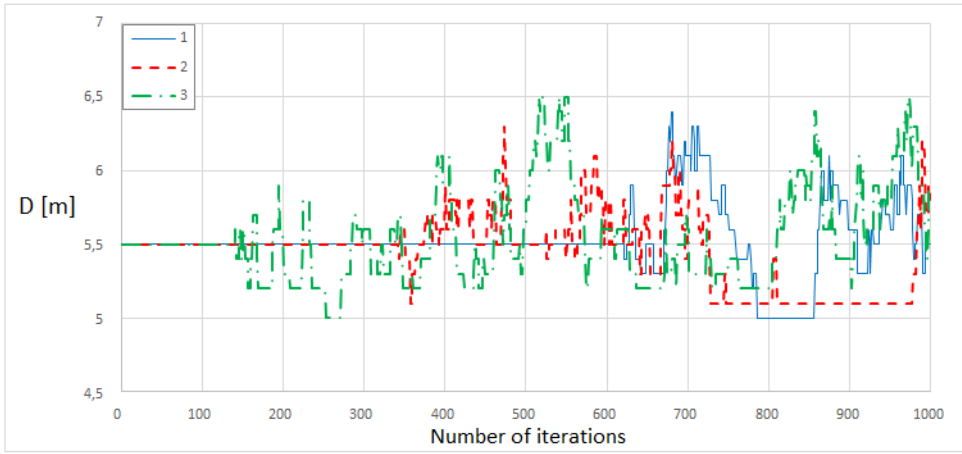

Figure 6.6: SA optimization I1 - Pile diameter, D, from three different calculations

Figure 6.7: SA optimization I1 - Probability of failure, P_f, from three different calculations

6.2.2 CPT Profile I4

As we see from Table 5.1 is the water depth at this location 18 m, Bolders Bank formation is 0-10 m below seabed, Egmond Ground 10-15 m and Swarte Bank from 15 m below seabed and down to the optimal penetration length of the monopile. The calculated correlation lengths from each layer and examples of random field realizations from this location is shown in appendix B.

Simulated Annealing

Seven calculations for CPT profile I4 was performed with the RBDO algorithm. Simulations of the algorithm with 1000 iteration were performed, and the SS was performed with 200 simulation per step. Figure 6.8 - 6.12 shows the calculated values of cost, L_p, w, D and P_F of the three first calculations. Table 6.3 shows the minimum costs and related parameters from each calculation.

Table 6.3: Optimal minimum costs for CPT profile I1 based on SA Optimization

N_s	Calculation number	$C(\mathbf{x},\mathbf{t})$	L_p	w	D	P_F
	[-]	[€]	[m]	[m]	[m]	[-]
200	1	$2.50x10^5$	26	0.04	4.9	6.8×10^{-5}
200	2	$2.85x10^5$	26	0.04	5.6	1.4×10^{-6}
200	3	$2.60x10^5$	26	0.04	5.2	3.5×10^{-5}
200	4	$2.76x10^5$	26	0.04	5.4	6.7×10^{-5}
200	5	$2.70x10^5$	26	0.04	5.3	1.4×10^{-5}
200	6	$2.70x10^5$	26	0.04	5.3	8.5×10^{-6}
200	7	$2.65x10^5$	26	0.04	5.2	4.0×10^{-5}

Table 6.3 show that the optimal design cost for these calculations is varying between $2.50 - 2.85x10^5$ €. The optimal pile wall thickness is consistently 0.04 m , L_p is 26 m and D is varying between 4.9-5.6 m. Figure 6.12 shows that the SA algorithm also satisfies the reliability constraint for the proposed design parameters at CPT profile I4.

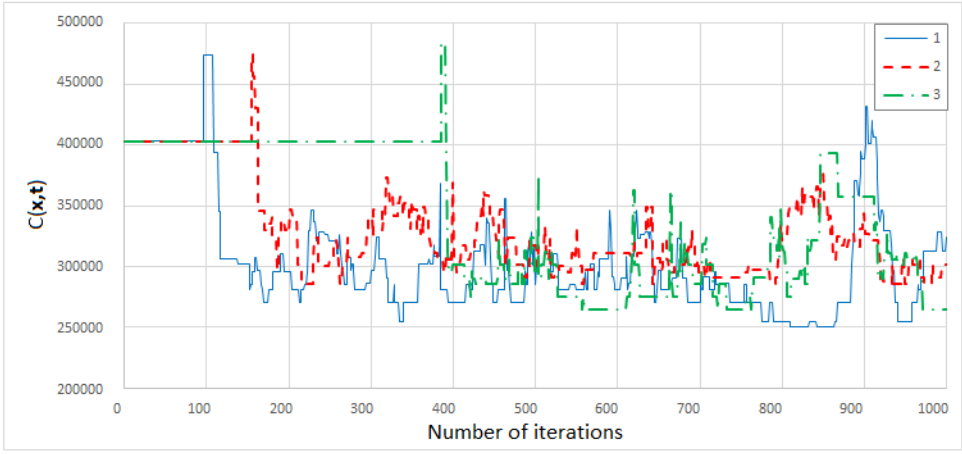

Figure 6.8: SA optimization I4 - Design cost of the monopile, C(**u,t**), from three different calculations

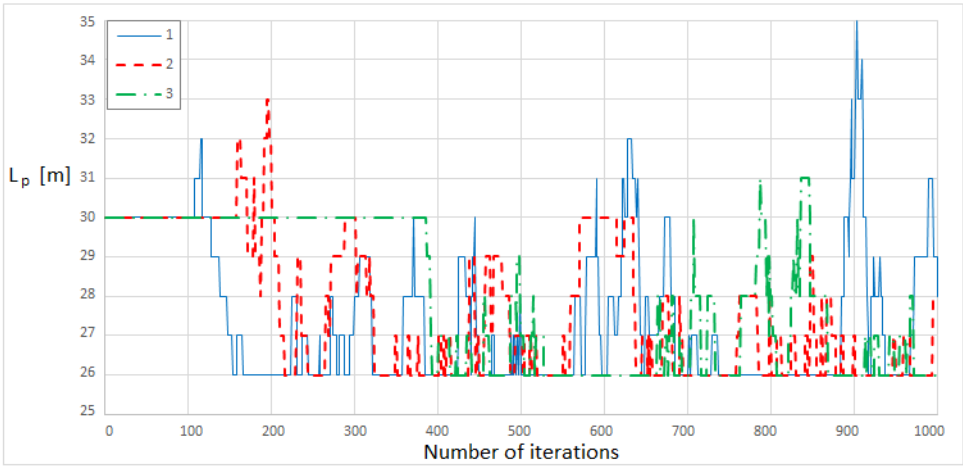

Figure 6.9: SA optimization I4 - Pile embedded length, L_p, from three different calculations

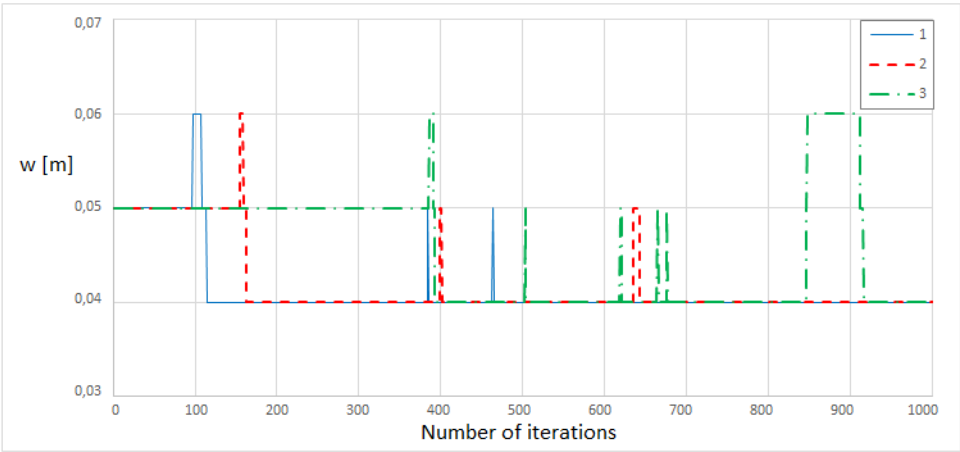

Figure 6.10: SA optimization I4 - Pile wall thickness, w, from three different calculations

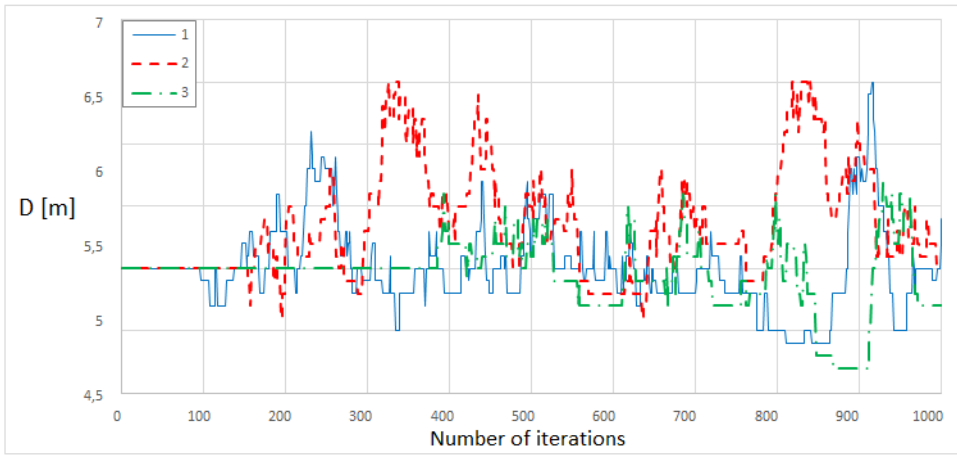

Figure 6.11: SA optimization I4 - Pile diameter, D, from three different calculations

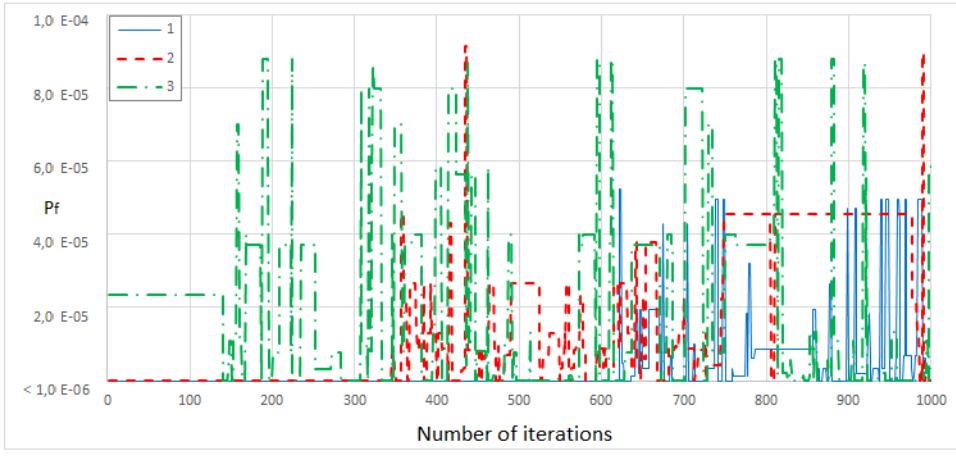

Figure 6.12: SA optimization I4 - Probability of failure, P_f, from three different calculations

Chapter 7

Discussion

This thesis is divided into four sections:

- Advanced estimation of random field parameters.
- Probabilistic soil parameter interpretation of CPT data.
- Integration with p-y curves.
- Reliability-based design optimization.

In chapter 6, the RBDO results are presented. To obtain these results, the effects of uncertainties must be included. How to estimate the random field parameters from CPT measurements was presented in chapter 4, and the probabilistic soil parameter interpretation was presented in chapter 5. These results are used to determine the random input variables for construction of p-y curves, which is described in section 5.4. To enlighten the importance of this, each section is discussed in this chapter.

7.1 Advanced Estimation of Random Field Parameters

In this study, tip resistance measured during CPT penetration is considered as a random field. The maximum likelihood method is used to estimate vertical correlation length, mean value and standard deviation. This advanced method estimates the optimal values of the random field parameters by maximizing the likelihood function.

The concept of a statistical dependence between field values at different location is expressed through the correlation length, which is one of the major features of a random field representation of soil properties. Figure 4.1 shows how the correlation length effects the value of the likelihood function. It can be observed that the maximum likelihood function is relatively flat between 0.7m-3m with the maximum around 1m. This indicates that the correlation length is not exactly 1m.

Fenton and Griffiths (2001) observed that the coefficient of variation of the bearing capacity is positively correlated with the spatial correlation length. Similar trend was observed in this study. Figure 7.1 shows how the correlation length at Bolders Bank formation tends to increase with higher coefficient of variation of the corrected tip resistance, q_t. Figure 7.2 shows that the data from Swarte Bank Formation have less correlation, but there is still some positively correlation between the correlation length and the coefficient of variation.

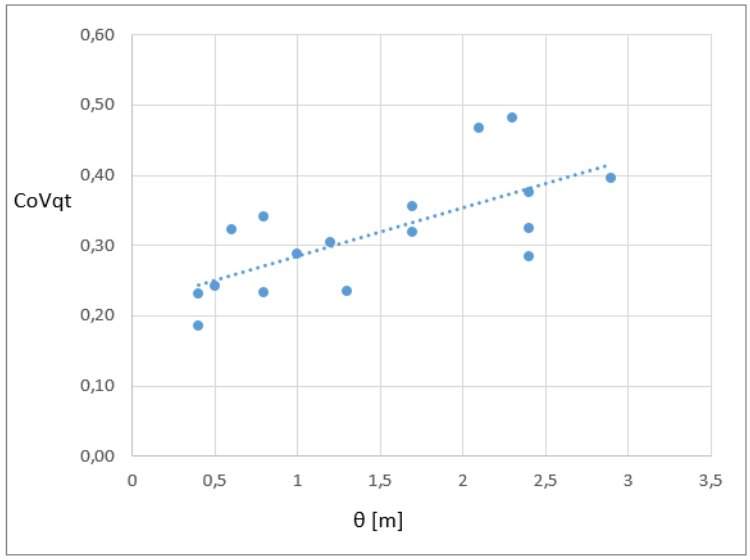

Figure 7.1: Correlation lengths from BDK plotted against coffiecient of variation for corrected cone tip resistance

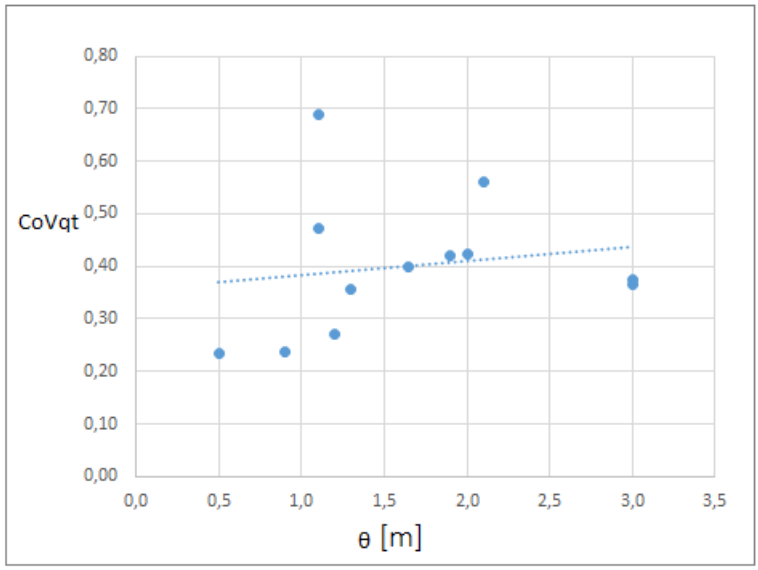

Figure 7.2: Correlation lengths from SBK plotted against coffiecient of variation for corrected cone tip resistance

Variation of the estimated values of the correlation length might come from different sources like measurement and modeling errors. How the boundaries for different soil layers are determined might also have a significant influence on the estimated correlation length. Which data that have been selected for further interpretation is important. Figure 7.3 shows how the value of θ slightly changes for different selected soil layer lengths. These correlation length are evaluated from CPT profile I1 from z= 1 m to z= 10 m . Even if the estimated value of θ is different, they all tend to reach a value of the likelihood function close to the maximum around θ = 0.7 m. When small layers are selected this results in dealing with limited data, and the estimated standard deviation would most likely be larger. This result in a higher coefficient of variation, which shown in Figure 7.1 may effect the value of the estimated correlation length.

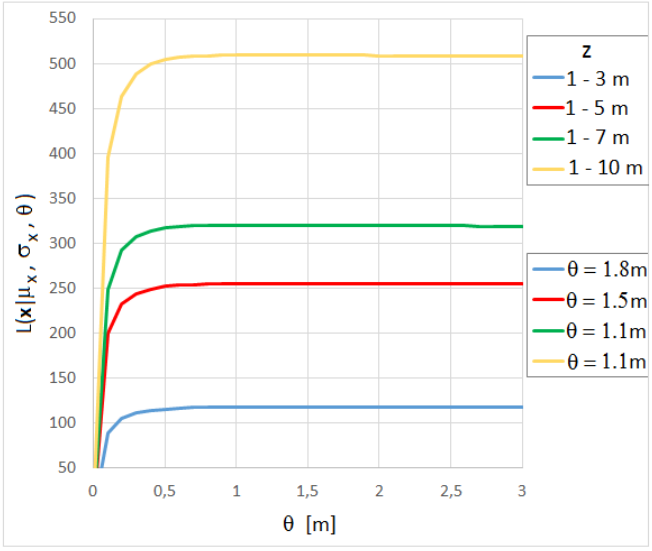

Figure 7.3: CPT profile I4 - Likelihood functions versus correlation length for different selected soil layer lengths

The Maximum likelihood approach showed reliable results for the probabilistic parameters of tip resistance measured during CPT, and provides a consistent framework to estimation of random field parameters for CPT data. The parameters were further used to develop a probabilistic interpretation of CPT data.

7.2 Probabilistic Interpretation of CPT Data

A probabilistic link between the CPT data and soil parameters is developed based on different interpretation techniques. The estimated parameters from the random field model of CPT measurements are further used to propose random fields of undrained shear strength and friction angle. Because these parameters are used to calculate the ultimate soil resistance, p_u, which is an important parameter for construction of p-y curves.

7.2.1 Undrained Shear Strength

The commonly used relation based on q_t was used to relate CPT measurement to an appropriate design parameter. One of the uncertainties about this approach is the determination of the probabilistic values of N_k. The uncertainty in this parameter could be reduced by some additional information.

The resulting S_u random fields from Bolders Bank Formation and Swarte Bank Formation were compared with values from the geotechnical report, and fit well with the suggested S_u profiles from Sheringham Shoal wind farm. These results indicates that the probabilistic interpretation of soil parameters based on a random field model of CPT data can be efficiently used to model variability of soil properties. The suggested profiles of S_u versus depth from Sheringham Shoal can be found in appendix A.

It can be observed that the random field profiles of S_u from SBK (Figure 6.2) exceed the upper estimate of the S_u profile from Sheringham Shoal wind farm. This is due to the large variance of the q_t random field at certain locations due to pockets of sand and gravel within the clay layer (e.g. Figure B.3).

7.2.2 Friction Angle

Robertson and Campanella (1983b) proposed a relationship between φ', q_c and σ'_{v0}. Based on the chart they developed, an equation to express how CPT measurement could be transformed to design parameters was established. Similar to the transformation uncertainty in S_u, also the transformation uncertainty in φ' is difficult to determine. The values selected for the transformation uncertainty was taken from Kulhawy and Mayne (1990), which established a similar transformation equation to the one used in this study.

The value of the friction angle was found to be 44° for the Edmond Ground Foundation (Saue and Meyer, 2009), and this value corresponded well with the mean value of the generated ϕ random field.

7.3 Integration with p-y Curves

The response of a monopile foundation to loads are simulated by the p-y model. In this model the pile is considered to be supported by a series of uncoupled non-linear springs. These non-linear springs, applied at the nodal points, are characterized by p-y curves and defines the material behavior at this point.

The variability of S_u and φ modeled by means of one-dimensional random field are expected to influence the pile-soil response. This is because S_u is directly related to the ultimate soil resistance, p_u, and p_u for sand is calculated by dimensionless coefficients which depends on the friction angle. The random fields are integrated in the p-y model to construct p-y curves, one for each nodal point. The interval length, $dl = \frac{L_p}{P}$, is set to 1 m .

Since the soil surrounding the pile was subdivided into three different layers, it is important to ensure that the correct p-y curve for each nodal point corresponds with the soil type surrounding it. When this is defined, the random field parameters estimated in chapter 5 are used to make new random field realizations with values for every 1 m . Based on soil type and depth, the p-y curve for each nodal point is created, and the stiffness matrix for the monopile is constructed. The p-y model provides a bending moment distribution from which the maximum stress in the pile can be determined.

The probabilistic models of soil parameters are coupled with the nonlinear p-y finite element model to evaluate the effect of local strength variation on the ultimate limit state of a monopile foundation.

7.4 Reliability-based Design Optimization

The last step in this study is to conduct a reliability-based design optimization (RBDO) to quantify uncertainties in soil parameters based on CPT investigations. Two different CPT profiles, I1 and I4, are presented to calculate the optimal design of a monopile foundation subjected to lateral loading.

7.4.1 Subset Simulation

The probability of exceeding the ultimate limit state is evaluated with the Subset Simulation (SS) method. In the SS algorithm special attention should be given to the failure probability convergence and the selection of the acceptance probability parameters. The calculations were performed with 200 simulations per iteration, and this number was selected to compromise between computational time and accuracy of the Subset Simulation. Due to the uncertainty in the estimate of failure probability and consequently the calculated design cost, several independent calculations of the RBDO algorithm were performed. Table 6.2 and 6.3 summarizes the results from these calculations. Due to uncertainty in the estimated failure probability there is some variability in the minimum cost estimates.

Once the RBDO estimate are obtained, a detailed examination is required. Table 6.2 and 6.3 shows that the algorithm tends to locate the same minimum for the design costs. L_p and w tends to have the same values for the optimal design, while the value of D is varying. The observed variation of D might be a result of the dominant effect of D on the probability of failure. This means that a slight variation of D might result in significant change in P_F, and a possible reliability constraint violation, $P_F(\mathbf{x},\hat{\mathbf{t}}) \geq P_F^{lim} = 10^{-4}$.

To increase the reliability of the proposed optimal design, a more accurate calculation for the failure probability can be performed. This might be done by increasing the numbers of simulations per iteration or by using other methods for calculating small failure probabilities.

The sensitivity of the pile-soil model to the soil and load variability is also investigated. The optimal solution of D=5.4 m, w=0.04 m and L_p=26 m from CPT profile I1 is selected for evaluation. The probability of failure for this design is calculated again to see how the random load and uncertainties in soil parameters affects the value of the performance function. The probability of failure was found to be $5.2x10^{-5}$ for this calculation, which is a result of 5 intermediate failure regions, F_i.

Effect of random load

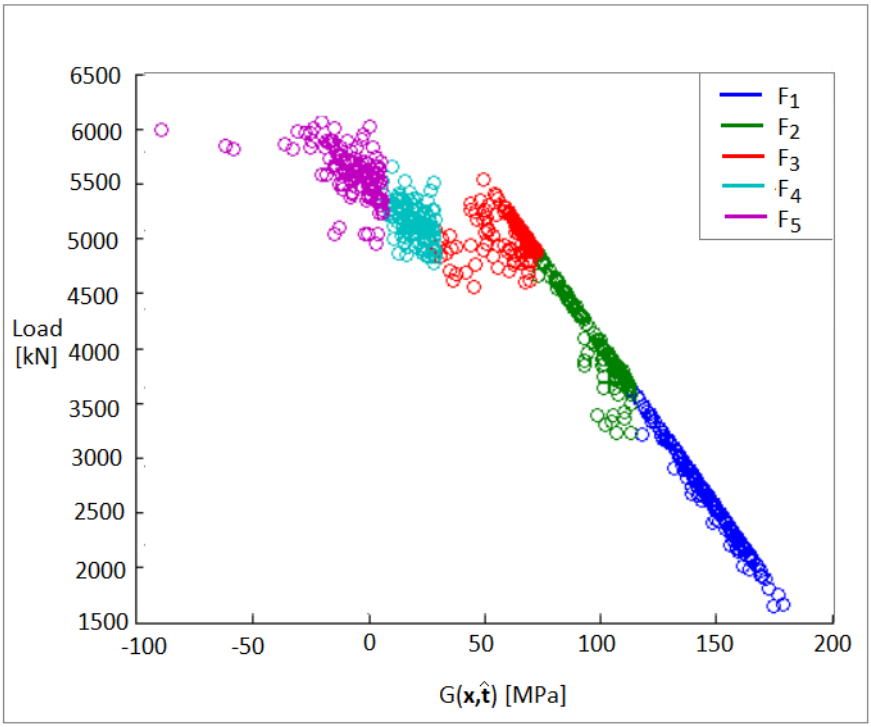

Figure 7.4: Random load plotted against performance function

Figure 7.4 shows that the random load is dominantly affecting the value of the performance function in first two intermediate failure regions. When the value of the performance function becomes smaller, it is likely to believe that the uncertainties in soil parameters becomes more significant.

Effect of S_u random field

For the optimal design values presented above, L_p was subdivided into 26 equally sized elements and represented by 27 non-linear springs at nodal points between the elements. To see how the S_u random field from BDK and SBK affects the value of the performance function it is possible to consider only one nodal point at the same time. The value of S_u from tow points is considered, one from each layer. For BDK, values from z=6 m are selected and for SBK values from

z=26m are selected. Figure 7.5 and 7.6 shows a scatter plot of S_u versus G($\mathbf{x},\hat{\mathbf{t}}$) from BDK and SBK respectively.

Values of S_u from BDK seems to correlate with the value of the performance function, particularly at low values. This indicates that the variability of S_u from BDK is affecting the probability of failure. These results are as expected, because lower values of S_u should give larger moments and higher stresses in the monopile, which results in a lower value of G($\mathbf{x},\hat{\mathbf{t}}$).

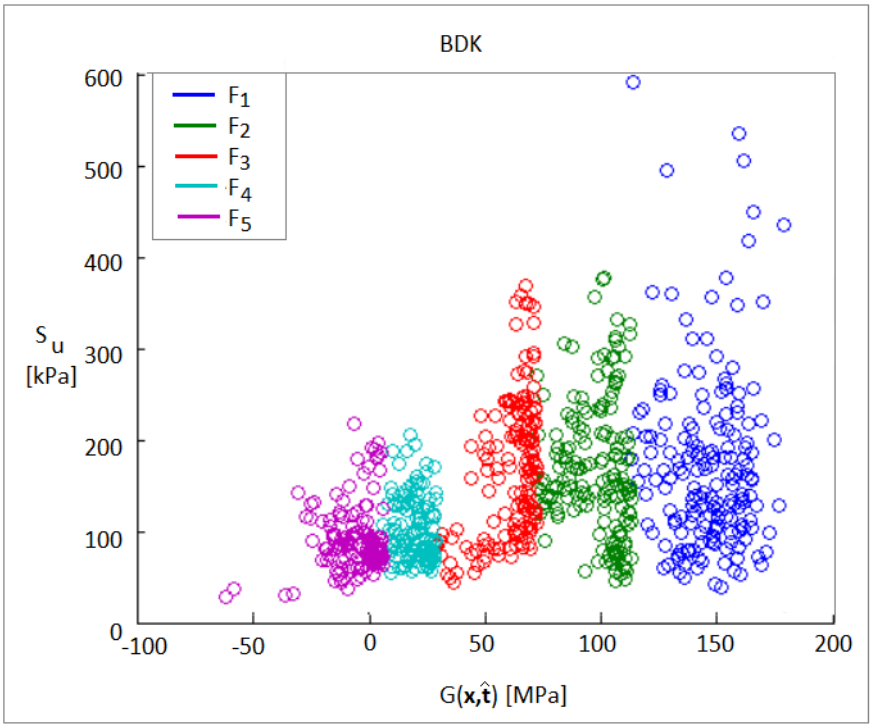

Figure 7.5: Su from one nodal point at BDK plotted against performance function

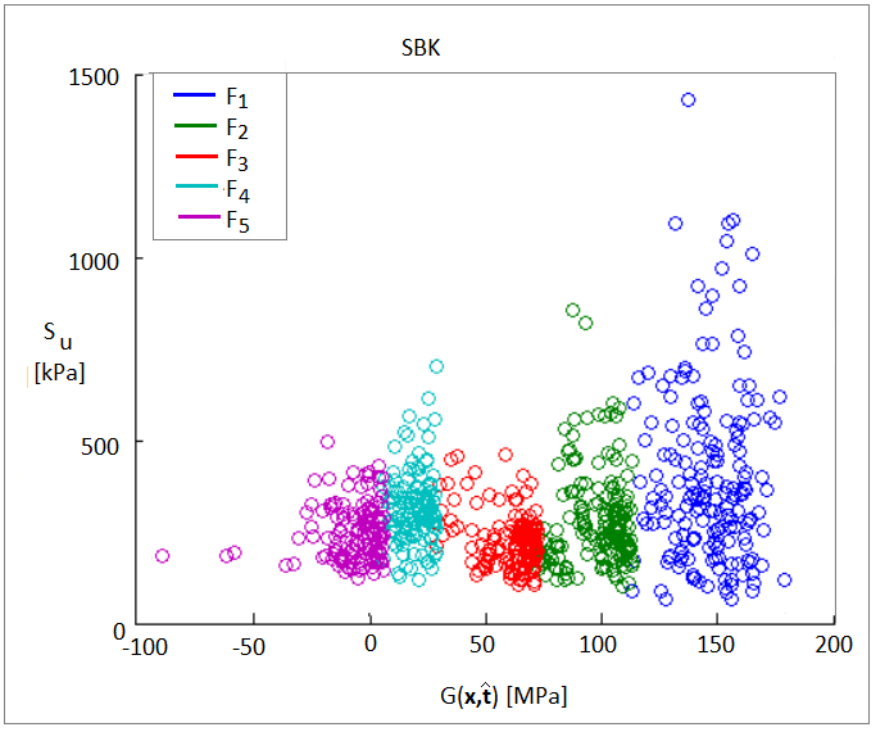

Figure 7.6: Su from one nodal point at SBK plotted against performance function

Effect of φ random field

Values from the φ random field is taken from z=16 m, and Figure 7.7 shows that the variability of φ does not significantly affect the value of the performance function. The location of the springs are also important, and in the middle of the pile will the effects of deformations be smaller. The sand layer is located from z=10 m to z =18 m, which is in the middle of the pile, and the results are as expected.

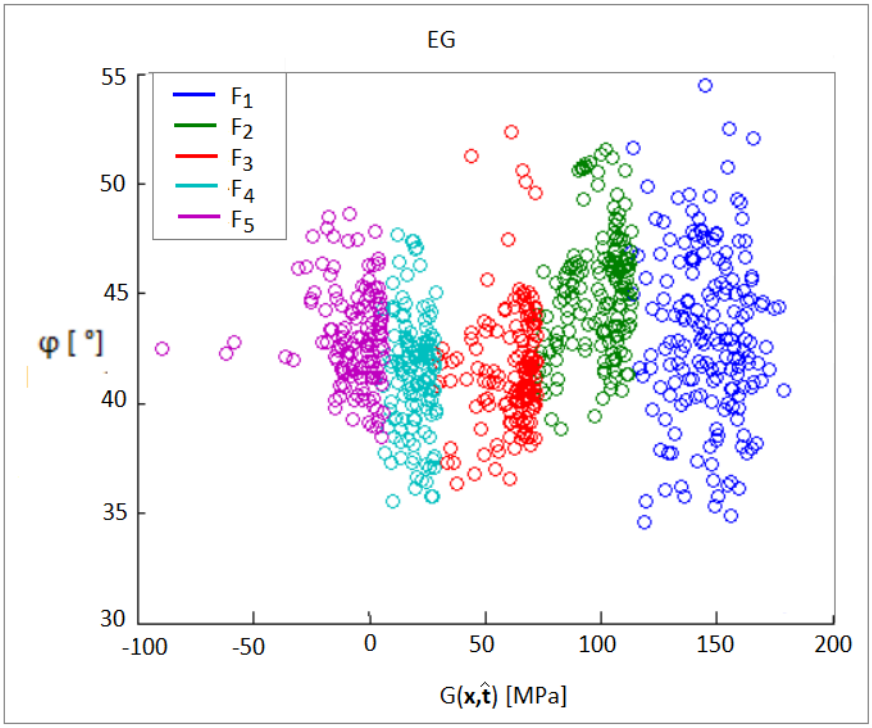

Figure 7.7: φ from one nodal point plotted against performance function

7.4.2 Simulated Annealing

As a stochastic optimization method, Simulated Annealing does not provide a convergence criteria that can guarantee that the located minimum from a number of simulations really is the global minimum. For this reason several independent optimization are calculated with the aim of location the global minimum.

Effect of Design Parameters

Figure 6.4 - 6.6 and 6.9 - 6.11 show that the value of D and L_p tend to vary more during the optimization process than the value of w. This indicates that the optimization process is sensitive to changes in w. Changes in w might easily result in increasing design cost or constraint violation. Figure 7.8 - 7.10 shows both the rejected and accepted values from the SA algorithm, and they support the state-

ment that design costs varies most with the pile wall thickness. Figure 7.9 shows that there is a strong correlation between pile wall thickness and design cost.

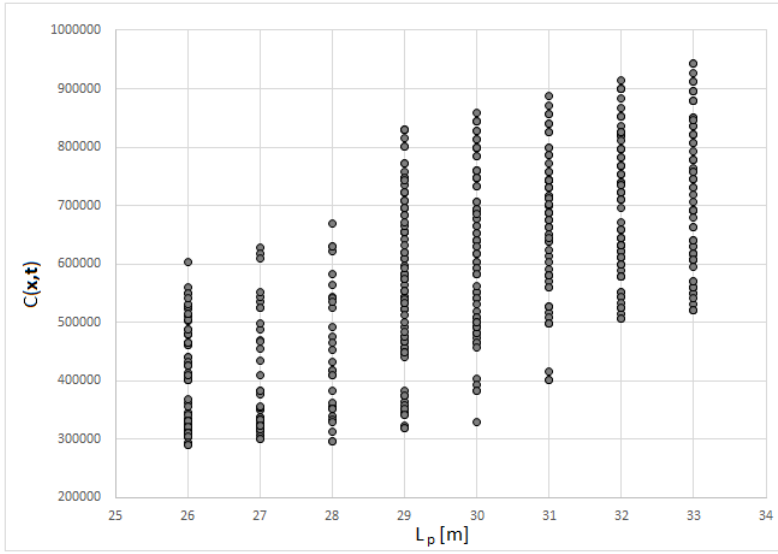

Figure 7.8: Design cost of monopile foundation plotted against pile penetration length, L_p

Figure 7.10 shows that there is no correlation between pile diameter and design cost. The red line in this figure indicates that the region to the left is probably the region where the reliability constraint is validated, which means that it is likely to believe that the diameter of the pile should be larger than 5.3 m to provide an optimal and safe design.

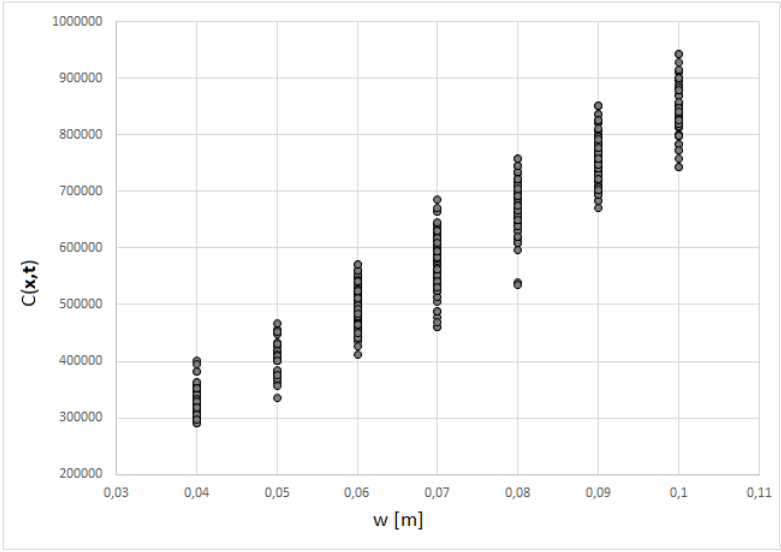

Figure 7.9: Design cost of monopile foundation plotted against pile wall thickness, w

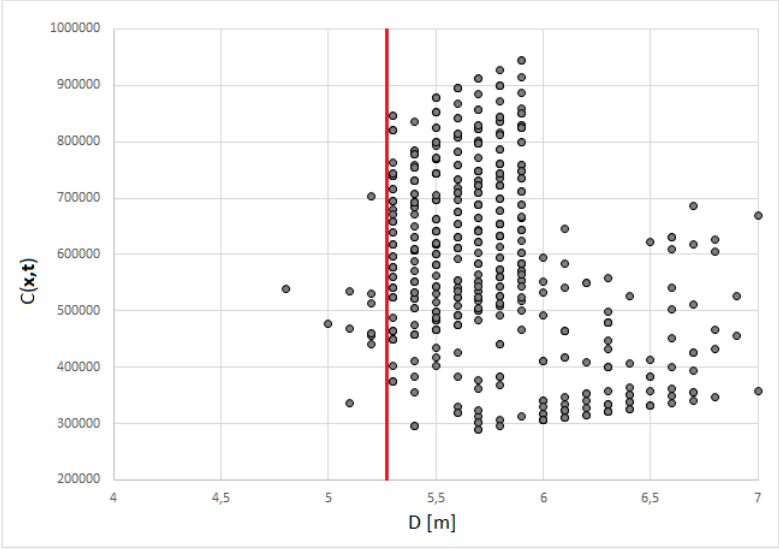

Figure 7.10: Design cost of monopile foundation plotted against pile diameter, D

7.4.3 RBDO and Geotechnical Engineering

In Geotechnical engineering it is of importance to provide answers about the reliability of a design, and this study shows an example of how probabilistic approaches can be integrated in design analyses. A RBDO has a large potential in geotechnical engineering and can be applied to give insight into the probability of exceeding a certain limit state as a probabilistic measure. Different limit states (e.g. ultimate limit state and serviceability limit state) for the same structure may give different consequences, and probabilistic approaches is thus sufficient for considering the consequences and optimizing the design for different limit states.

The initial values of the design parameters in the SA algorithm were set to D=5.5 m, w=0.05 m and L_p=30 m, which gave a probability of failure $P_F(\mathbf{x},\hat{\mathbf{t}}) < 10^{-6}$ and design costs $C(\mathbf{x},\hat{\mathbf{t}}) = 4.03\times10^5$ €. These values were based on an initial engineering guess. By using the SA algorithm the cost from the proposed initial design was reduced with approximately 30 %.

Monopile foundations is an example of structures where the area exposed to soil is small compared to other foundation design, and uncertainties associated with soil properties requires a special consideration. The local strength variation was expected to influence the pile-soil response. In this study, the probability of failure was dominantly related to the uncertainties of random load, as shown in Figure 7.4, but the uncertainty in S_u did also effect the value of the performance function significantly. Results in Figure 7.4 - 7.7 illustrate the significance of parameters uncertainty, and this is one of the great advantages by using probabilistic approaches. Results of a probabilistic analysis can indicate a relative contribution to the resulting random response. These observations can further be used to investigate or reduce uncertainty associated with random parameters. E.g. if the values from the S_u random fields tended to affect the probability of failure significantly, further field investigations could be performed to reduce some of the uncertainty in this parameter.

Chapter 8

Summary and Recommendations for Further Work

8.1 Summary and Conclusions

In deterministic geotechnical design, characteristic values and the factor of safety approach are commonly used to maintain some degree of safety. The main concern behind this approach is that it does not give a completely indicator of the safety margin, because it does not explicitly account for the effects of uncertainties. How the uncertainties in soil parameters and loads affect the reliability of a geotechnical design is important, and probabilistic approaches becomes more necessary for design analyses when the level of uncertainty is high. The uncertainty can not be removed by using reliability approaches, but they do provide a way of handling them consistently.

A Reliability-based design optimization (RBDO) is a design methodology that accounts for the effects of uncertainties on the structural reliability while searching for a design which minimizes structural performance criteria (e.g. cost). The goal for the RBDO in this study is to optimize cost of construction, installation and failure while accounting for the effects of uncertainties in soil parameters and lateral load on the reliability of a monopile foundation. The response of a monopile foundation subjected to lateral loading was evaluated with respect to the ultimate limit state, defined by the yield strength of the monopile steel.

Uncertainty due to inherent soil variability, measurement errors and mod-

eling assumptions are described by the random field model. The random field model for soil parameters and uncertainties related to lateral load was coupled with the nonlinear p-y finite element model to predict the response of a monopile foundation. The variability of S_u and φ were expected to influence the pile-soil response significantly, and a probabilistic interpretation from CPT measurement was conducted for these soil parameters.

Gaussian random fields were used to describe soil conditions in a probabilistic manner based on observed and measured data. This method is preferred, because statistical dependence between field values at different points is expressed through the correlation length. By comparing the generated random fields of design parameters with existing suggested estimates, it is reasonable to assume that the random fields represent the variability of soil conditions in a good way.

RBDO algorithm, which couples the Subset Simulation reliability (SS) method with the Simulated Annealing (SA) stochastic optimization algorithm, was used to achieve an efficient and accurate optimization process. The SS algorithm was used to calculate the probability of exceeding the ultimate limit state, and the SA algorithm ensured that proposed design parameters were rejected if $P_F(\mathbf{x},\hat{\mathbf{t}}) \geq P_F^{lim} = 10^{-4}$.

The results from the SA algorithm indicate that the method can be considered as robust and efficient for standardized structural design of monopile foundations subjected to static lateral loading. Each calculation gave almost the same result, which indicates that it is likely to believe that the global optimal minimum is within this area. Some consideration should be given to the calculation of failure probability, due to the selected numbers of simulations and acceptance probability parameter.

This study shows that a RBDO can provide an optimal selection of design variables while explicitly accounting for the effects of uncertainties. In addition to optimal design it provides an insight into the likelihood of exceeding the limit state as a probabilistic measure. The economical design can thus be optimized by achieving a proper balance among initial cost, risk of failure and consequences of failure.

8.2 Recommendations for Further Work

It would be interesting to use other reliability methods and alternative algorithms to perform a RBDO for this geotechnical design. To determine soil layer boundaries, a more accurate CPT classification system could have been implemented to see if it is possible to reduce some of the variation of the estimated cone tip resistance.

In this study, the ultimate limit state defined by the steel yield stress was evaluated. Other limit states, such as serviceability limit state and fatigue limit state, would also be interesting to investigate. More advanced finite element methods could also be performed to calculate the pile-soil response.

To strengthen the credibility of the results in this study, a design based on well known deterministic geotechnical approaches should be performed. This can be done by calculating a factor of safety for the optimal reliability-based design based on characteristic values for soil parameters and load.

Bibliography

Aas, G., Lacasse, S., Lunne, T., and Hoeg, K. (1986). Use of in situ tests for foundation design on clay. *Publikasjon-Norges Geotekniske Institutt*, (166):1–15.

Achmus, M., Kuo, Y.-S., and Abdel-Rahman, K. (2009). Behavior of monopile foundations under cyclic lateral load. *Computers and Geotechnics*, 36(5):725–735.

Agarwal, P. and Manuel, L. (2009). On the modeling of nonlinear waves for prediction of long-term offshore wind turbine loads. *Journal of Offshore Mechanics and Arctic Engineering*, 131(4):041601.

API, R. (2011). 2geo. *Geotechnical and Foundation Design Considerations-*.

Au, S.-K. and Beck, J. L. (2001). Estimation of small failure probabilities in high dimensions by subset simulation. *Probabilistic Engineering Mechanics*, 16(4):263–277.

Baecher, G. B. and Christian, J. T. (2005). *Reliability and statistics in geotechnical engineering*. John Wiley & Sons.

Breton, S.-P. and Moe, G. (2009). Status, plans and technologies for offshore wind turbines in europe and north america. *Renewable Energy*, 34(3):646–654.

Depina, I. and Eiksund, G. R. (2015). Reliability-based design optimization of laterally loaded monopile foundations for offshore wind turbines.

DNV (2010). Dnv-os-j101 offshore standard. *Design of Offshore Wind Turbine Structures*.

Doherty, P. and Gavin, K. (2012). Laterally loaded monopile design for offshore wind farms.

Fenton, G. A. and Griffiths, D. (2001). Bearing capacity of spatially random soil: the undrained clay prandtl problem revisited. *Geotechnique*, 51(4):351–359.

Fenton, G. A. and Griffiths, D. V. (2008). *Risk Assessment in Geotechnical Engineering*. Wiley Online Library.

Goffe, W. L., Ferrier, G. D., and Rogers, J. (1994). Global optimization of statistical functions with simulated annealing. *Journal of Econometrics*, 60(1):65–99.

Huber, M. (2013). Soil variability and its consequences in geotechnical engineering. Technical report, Institut für Geotechnik der Universität Stuttgard.

Karlsrud, K., Lunne, T., and Brattlien, K. (1997). Improved cptu interpretations based on block samples. *Publikasjon-Norges Geotekniske Institutt*, 202:195–201.

Klüppelberg, C., Straub, D., and Welpe, I. M. (2014). Risk–a multidisciplinary.

Kulhawy, F., Birgisson, B., and Grigoriu, M. (1992). Reliability-based foundation design for transmission line structures. Technical report, Electric Power Research Inst., Palo Alto, CA (United States); Cornell Univ., Ithaca, NY (United States). Geotechnical Engineering Group.

Kulhawy, F. H. and Mayne, P. W. (1990). Manual on estimating soil properties for foundation design. Technical report, Electric Power Research Inst., Palo Alto, CA (USA); Cornell Univ., Ithaca, NY (USA). Geotechnical Engineering Group.

Lacasse, S. and Nadim, F. (1997). Uncertainties in characterising soil properties. *Publikasjon-Norges Geotekniske Institutt*, 201:49–75.

LeBlanc, C. (2009). *Design of offshore wind turbine support structures*. PhD thesis, Department of Civil Engineering, Aalborg University, Denmark.

Liu, C.-N. and Chen, C.-H. (2010). Estimating spatial correlation structures based on cpt data. *Georisk*, 4(2):99–108.

Lunne, T., Eide, O., and Ruiter, J. d. (1976). Correlations between cone resistance and vane shear strength in some scandinavian soft to medium stiff clays. *Canadian geotechnical journal*, 13(4):430–441.

Lunne, T., Robertson, P., and Powell, J. (1997). Cone penetration testing. *Geotechnical Practice*.

O'Neill, M. W. and Murchison, J. M. (1983). *An evaluation of py relationships in sands*. University of Houston.

Phoon, K.-K. and Kulhawy, F. H. (1999). Evaluation of geotechnical property variability. *Canadian Geotechnical Journal*, 36(4):625–639.

Rad, N. and Lunne, T. (1989). Direct correlations between piezocone test results and undrained shear strength of clay. *Norwegian Geotechnical Institute Publication*, (177).

Reese, L. C., Cox, W. R., Koop, F. D., et al. (1975). Field testing and analysis of laterally loaded piles om stiff clay. In *Offshore Technology Conference*. Offshore Technology Conference.

Robertson, P. and Campanella, R. (1983a). Interpretation of cone penetration tests. part ii: Clay. *Canadian Geotechnical Journal*, 20(4):734–745.

Robertson, P. K. and Campanella, R. (1983b). Interpretation of cone penetration tests. part i: Sand. *Canadian Geotechnical Journal*, 20(4):718–733.

Ronold, K. O. (1990). Random field modeling of foundation failure modes. *Journal of geotechnical engineering*, 116(4):554–570.

Saue, M. and Meyer, V. (2009). Geotechnical report: Sheringham shoal wind farm soil investigation (20081313-1). *Oslo, Norway: Norwegian Geotechnical Institute (NGI)*.

Sorensen, J. D. and Tarp-Johansen, N. J. (2005). Reliability-based optimization and optimal reliability level of offshore wind turbines. *International Journal of Offshore and Polar Engineering*, 15(2):141–146.

Sørensen, S. P. H., Brødbæk, K. T., Møller, M., and Augustesen, A. H. (2012). Review of laterally loaded monopiles employed as the foundation for offshore

wind turbines. Technical report, Department of Civil Engineering, Aalborg University.

Van Laarhoven, P. J. and Aarts, E. H. (1987). *Simulated annealing*. Springer.

Appendix A

Sheringham Shoal Wind Farm

A.1 Undrained Shear Strength

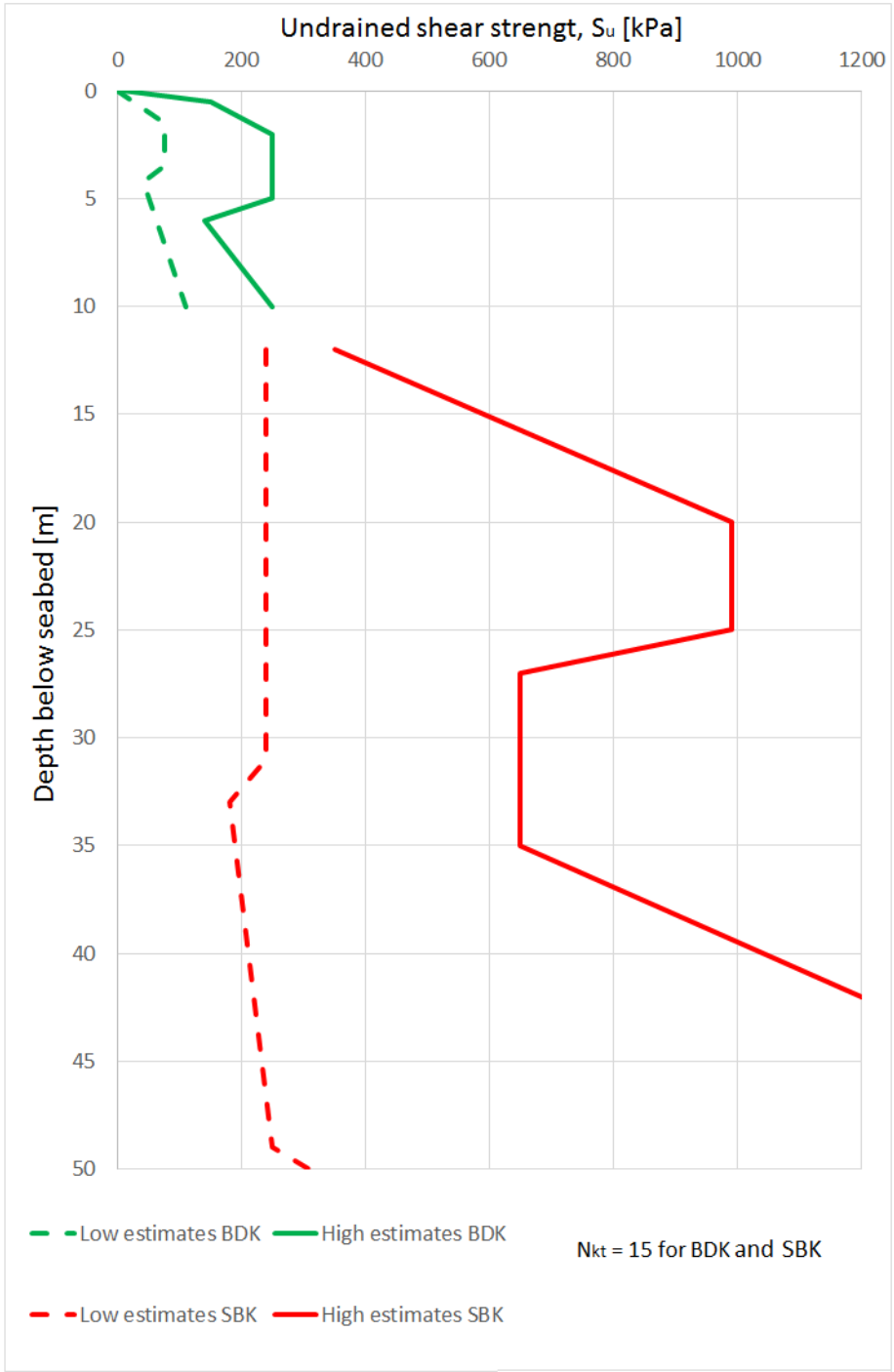

Figure A.1: Suggested estimates of S_u versus depth (after Saue and Meyer, 2009)

Appendix B

Parameters from different CPT Profiles

B.1 Bolders Bank Formation

B.1.1 Selected Soil Layers

CPTU	Water depth [m]	Depth below seabed [m]	Length [m]
A3	15,5	2,0 - 7,4	5,4
A4	15,5	0,5 - 8,4	7,9
B1	15,0	0,7 - 9,0	8,3
B2	15,5	2,0 - 9,0	7,0
C1	15,0	1,0 - 12,5	11,5
C1A	15,0	0,6 - 9,0	8,4
C2	15,5	0,6 - 9,5	8,9
C4A	18,0	1,5 - 7,0	5,5
C7	19,0	0,7 - 7,0	6,3
D3	16,5	0,6 - 10,5	9,9
D4	18,0	0,6 - 7,0	6,4
E1	16,0	0,7 - 9,0	8,3
H5	19,0	2,0 - 8,0	6,0
I6	19,0	0,7 - 9,0	8,3
J2	17,5	1,5 - 9,5	8,0
J6	18,0	2,0 - 8,0	6,0
K2	18,0	2,0 - 7,0	5,0
Mean			

Table B.1: Selected soil layers from BDK for interpretation of CPT measurements

B.1.2 Parameters for Construction of Su Random Fields

CPTU	θ [m]	μqt [MPa]	σqt [MPa]	CoVqt	α_1	α_2	β_1 [10^{-3}]	β_2
A3	0,4	1,68	0,39	0,23	-0,016	-2,3	2,4	0,42
A4	1,0	2,08	0,60	0,29	-0,013	-2,0	2,4	0,46
B1	2,1	1,50	0,70	0,47	-0,021	-2,5	6,6	0,60
B2	0,5	1,86	0,45	0,24	-0,014	-2,1	2,7	0,46
C1	1,3	1,87	0,44	0,24	-0,014	-2,1	2,2	0,42
C1A	2,4	1,84	0,69	0,38	-0,016	-2,2	4,0	0,52
C2	0,8	1,79	0,61	0,34	-0,016	-2,2	3,9	0,50
C4A	2,4	1,94	0,55	0,28	-0,014	-2,1	2,7	0,46
C7	2,4	2,00	0,65	0,33	-0,014	-2,1	3,1	0,49
D3	1,7	1,91	0,61	0,32	-0,015	-2,1	3,2	0,48
D4	2,3	1,62	0,78	0,48	-0,020	-2,4	6,2	0,61
E1	0,4	1,83	0,34	0,19	-0,014	-2,2	1,6	0,40
H5	2,9	2,22	0,88	0,40	-0,013	-2,0	3,5	0,54
I6	0,8	1,97	0,46	0,23	-0,014	-2,1	2,1	0,42
J2	1,7	2,22	0,79	0,36	-0,013	-2,0	3,1	0,51
J6	1,2	1,81	0,55	0,30	-0,016	-2,2	3,3	0,47
K2	0,6	1,95	0,63	0,32	-0,014	-2,1	3,2	0,49
Mean	1,5	1,89	0,60	0,32	-0,015	-2,2	3,3	0,49

Table B.2: Calculated values from BDK to use as input parameters in random fields

B.2 Swarte Bank Formation

B.2.1 Selected Soil Layers

CPTU	Water depth [m]	Depth below seabed [m]	Length [m]
A7	20,0	17,0 - 24,0	7,0
C6	19,5	17,0 - 24,0	7,0
D6	20,0	16,6 - 28,7	12,1
E8	22,0	18,5 - 27,2	8,7
F6	20,0	18,0 - 27,0	9,0
G6	19,0	14,1 - 27,1	13,0
H1	18,0	18,1 - 23,2	5,1
I1	17,5	20,0 - 28,4	8,4
I4	18,5	16,5 - 27,0	10,5
I6	19,0	16,7 - 33,0	16,3
J6	18,5	13,2 - 25,5	12,3
Mean			

Table B.3: Selected soil layers from SBK for interpretation of CPT measurements

B.2.2 Parameters for Construction of Su Random Fields

CPTU	θ [m]	μqt [MPa]	σqt [MPa]	CoVqt	α_1	α_2	β_1 [10^{-3}]	β_2
A7	2,0	5,98	2,53	0,42	-0,0046	-0,98	1,30	0,54
C6	3,0	9,75	3,55	0,36	-0,0026	-0,46	0,60	0,49
D6	0,9	9,57	2,26	0,24	-0,0025	-0,44	0,34	0,41
E8	0,5	10,38	2,44	0,24	-0,0023	-0,36	0,31	0,41
F6	1,9	5,99	2,51	0,42	-0,0047	-0,98	1,30	0,54
G6	3,0	9,46	3,54	0,37	-0,0027	-0,49	0,64	0,50
H1	1,1	7,02	4,84	0,69	-0,0045	-0,93	1,60	0,72
I1	2,1	10,79	6,04	0,56	-0,0027	-0,43	0,86	0,63
I4	1,1	8,79	4,16	0,47	-0,0031	-0,60	0,90	0,57
I6	1,2	6,81	1,85	0,27	-0,0037	-0,79	0,64	0,44
J6	1,3	9,84	3,52	0,36	-0,0026	-0,44	0,57	0,49
Mean	1,6	8,58	3,39	0,40	-0,0033	-0,63	0,82	0,52

Table B.4: Calculated values from SBK to use as input parameters in random fields

B.3 CPT Profile I1

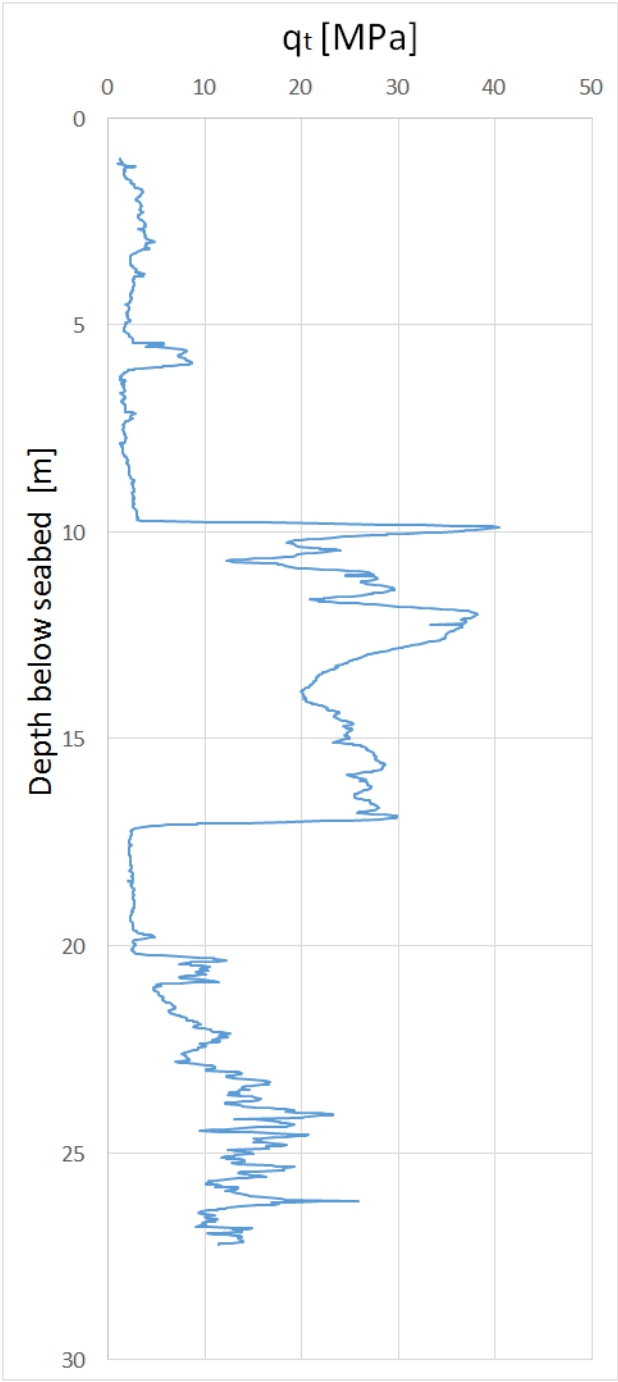

Figure B.1: Corrected cone resistance, q_t, versus depth for CPT profile I1

B.4 CPT Profile I4

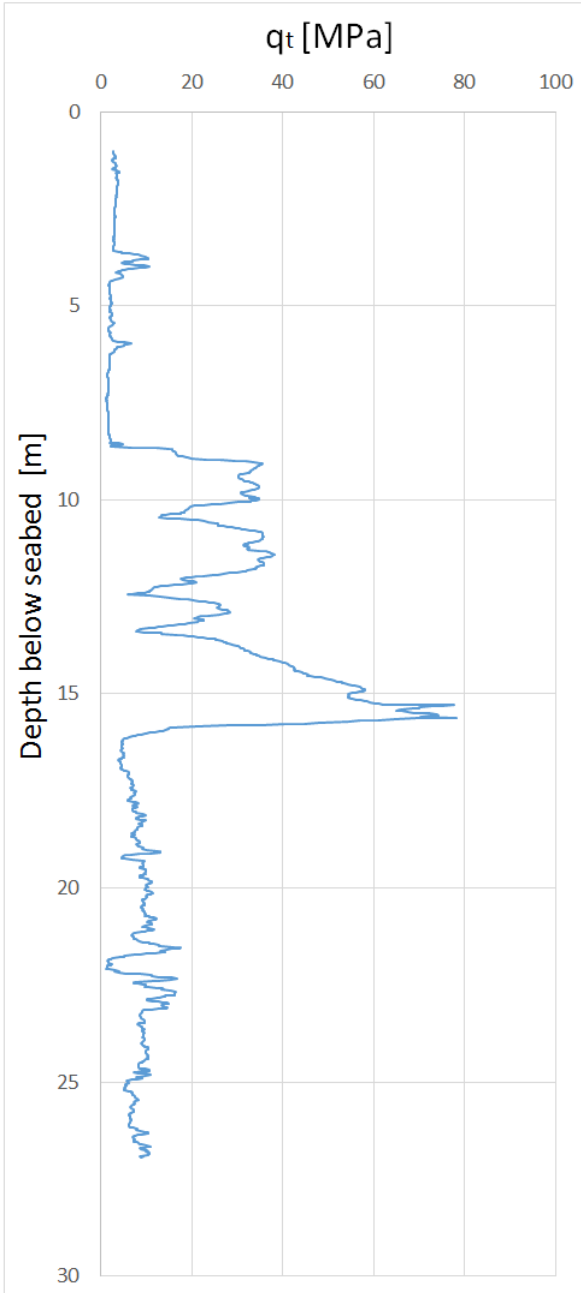

Figure B.2: Corrected cone resistance, q_t, versus depth for CPT profile I4

B.4.1 Random Fields of S_u and ϕ

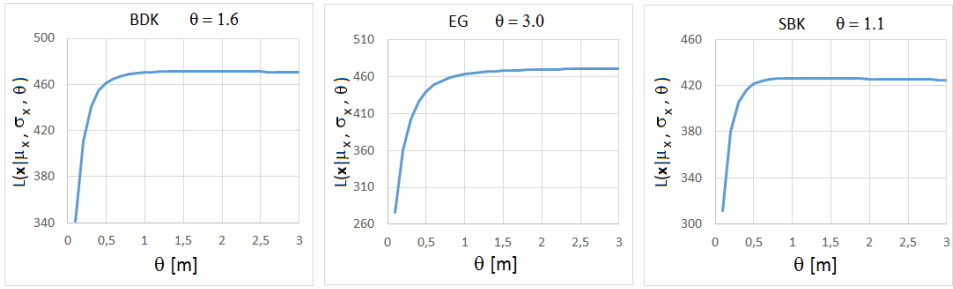

Figure B.3: Makimum likelihood estimates of correlation length for layers at CPT profile I4

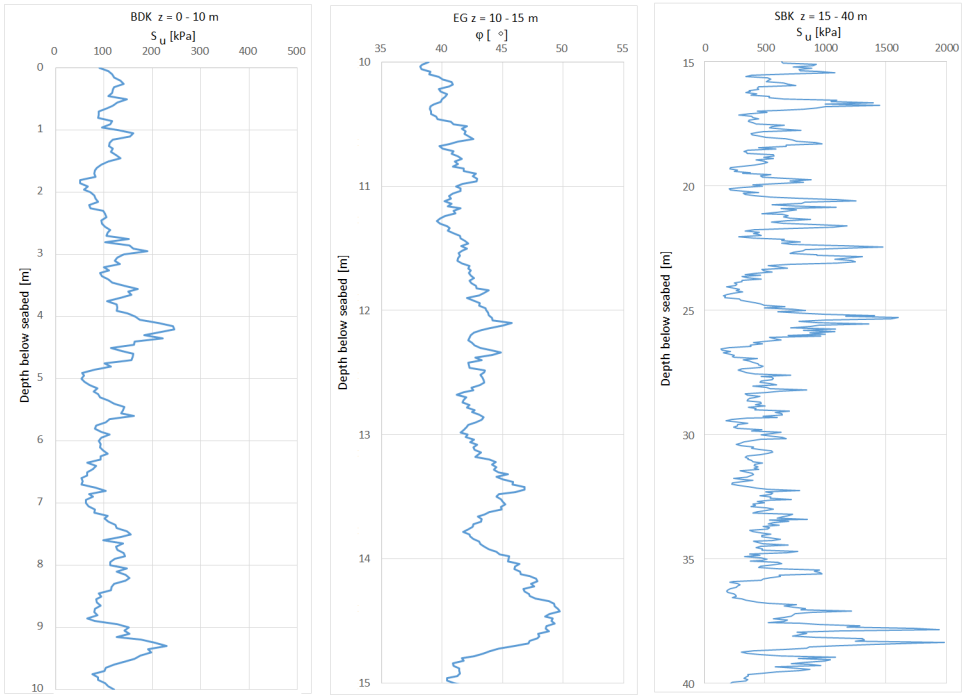

Figure B.4: Random field realizations for CPT profile I4